THE EFFECT OF TANGENTIAL GAS VELOCITY ON COMBUSTION INSTABILITY IN A LIQUID-GAS COMBUSTOR

Donald William Avery

NAVAL POSTGRADUATE SCHOOL
Monterey, California

THESIS

THE EFFECT OF TANGENTIAL GAS VELOCITY ON COMBUSTION INSTABILITY IN A LIQUID-GAS COMBUSTOR

by

Donald William Avery Jr.

Thesis Advisor: D. W. Netzer

December 1971

Approved for public release; distribution unlimited.

The Effect of Tangential Gas Velocity
On Combustion Instability
In a Liquid-Gas Combustor

by

Donald William Avery, Jr.
Lieutenant Commander, United States Navy
B.S., Tufts University, 1963

Submitted in partial fulfillment of the
requirements for the degree of

AERONAUTICAL ENGINEER

from the

NAVAL POSTGRADUATE SCHOOL
December 1971

ABSTRACT

A small, uncooled liquid rocket motor was utilized to examine the effects of the magnitude and direction of a steady vortex velocity on combustion instability. The rocket operated on normal heptane and air, with air flow rates controllable to allow for various amounts of tangential momentum.

Results of this investigation indicated that an energy feedback mechanism, through tangential momentum, did exist for both tangential and radial modes of instability. It was further shown that limit values of tangential velocity did exist, for a particular combustor, above and below which instability did not occur.

TABLE OF CONTENTS

I. INTRODUCTION -- 10

II. GENERAL DISCUSSION OF THE PROBLEM ------------- 13

III. EXPERIMENTAL APPROACH --------------------------- 17

IV. DESCRIPTION OF APPARATUS ---------------------- 21

- A. GENERAL ------------------------------------- 21
- B. ROCKET MOTOR ------------------------------ 21
- C. FUEL SUPPLY SYSTEM ----------------------- 22
- D. AIR SUPPLY SYSTEM ------------------------- 23
- E. IGNITION ------------------------------------- 25
- F. INSTRUMENTATION ---------------------------- 25

V. RESULTS -- 29

VI. DISCUSSION OF RESULTS ---------------------------- 36

VII. CONCLUSIONS --- 45

LIST OF REFERENCES -------------------------------------- 80

INITIAL DISTRIBUTION LIST ------------------------------ 82

FORM DD 1473 --- 83

LIST OF TABLES

Table Page

I. INSTRUMENTATION ---------------------------------- 26

II. DATA SUMMARY ------------------------------------- 30

LIST OF FIGURES

Figure Page

1. Instability Boundaries for a Vaporization Model with Vortex Flow ------------------------ 47

2. Instability Boundaries for Vaporization Model -- 48

3. Phase Relations for Spinning Transverse Waves -- 49

4. Air Swirl Plates and Insert Elements ---------- 50

5. Rocket Motor Configured for Cold Flow Data ---- 51

6. Rocket Motor on Thrust Stand ------------------ 52

7a. Control Console A ----------------------------- 53

7b. Control Console B ----------------------------- 53

8. Data Acquisition Panel ------------------------ 54

9. Rocket Motor ---------------------------------- 55

10. Rocket Nozzle --------------------------------- 56

11. High Frequency Pressure Instrumentation and Photographic Windows -------------------------- 57

12. Propellant Supply System ---------------------- 58

13. Fuel and Air Supply System -------------------- 59

14. Fuel Control Console -------------------------- 60

15. Fuel Injector --------------------------------- 61

16. Air Injector Manifold ------------------------- 62

17. Air Injector Manifold ------------------------- 63

18. Fuel Injector --------------------------------- 64

19. Ignition System ------------------------------- 65

20. Igniter -- 66
21. Igniter -- 67
22. Rocket Ignition Control ---------------------- 68
23. Signal Conditioner --------------------------- 69
24. Mixture Ratio vs. Characteristic Exhaust Velocity -- 70
25. Velocity Profile with 20-Degree Inserts ------ 71
26. Velocity Profile with 40-Degree Inserts ------ 72
27. Typical Visicorder Output -------------------- 73
28. High Frequency Data Output ------------------- 74
29. High Frequency Data Output (Expanded Time Scale) -- 75
30. Combustion Efficiency vs. P_p ---------------- 76
31. Mixture Ratio vs. P_p ------------------------- 77
32. Tangential Gas Velocity vs. P_p --------------- 78
33. Tangential Momentum vs. P_p ------------------ 79

TABLE OF SYMBOLS AND ABBREVIATIONS

$\mathcal{A}$	Combustor Contraction Ratio $[\frac{A_c}{A_t}]$
A_c	Cross Sectional Area of Combustor
A_t	Nozzle Throat Area
CCW	Counterclockwise Secondary Airflow
CW	Clockwise Secondary Airflow
c*	Characteristic Exhaust Velocity
g	Gravitational Constant
$\mathcal{L}$	Burning Rate Parameter $[\frac{Rm}{\mathcal{A}}]$
m	Average Burning Rate of Propellant per Length of Combustor
$P_{c_{max}}$	Maximum Chamber Pressure
$P_{c_{min}}$	Minimum Chamber Pressure
$P_{c,o}$	Steady State Chamber Pressure
$\dot{M}$	Propellant Weight Flow Rate
P_p	Non-dimensional Peak-to-Peak Pressure Disturbance $[\frac{P_{c_{max}} - P_{c_{min}}}{P_{c,o}}]$
R	Radius of Combustor
ST	Straight Secondary Airflow
T	Combustion Gas Temperature
V	Velocity of Chamber Gases
V_θ	Tangential Gas Velocity

1R	First Radial Instability
2T	Second Tangential Instability
1T	First Tangential Instability
S1T	Spinning First Tangential Instability
η_{c^*}	Combustion Efficiency $[\frac{c^*}{c^*_{theo}}]$
ΔV	Velocity difference between liquid and gas $(\Delta V_R{}^2 + \Delta V_\theta{}^2)^{1/2}$
φ	Ratio of tangential to total momentum

ACKNOWLEDGEMENTS

The author expresses his gratitude to Dr. David W. Netzer through whose guidance, encouragement, and direction this research effort was made possible.

The author is thankful to Mr. Edward Michelson for his cheerful assistance throughout the project, to Mr. Cecil R. Gordon for his numerous electronics contributions to the system, and to Mr. Frank Abbey and Mr. Glenn Middleton for their construction of system components.

A special note of gratitude goes to my wife, Sandra, for her patience and understanding.

I. INTRODUCTION

Liquid propellant rocket engines almost inevitably encounter the problem of combustion instability at some time during engine development. In the past two decades a number of combustion instability models have emerged in an attempt to accurately predict instability boundaries.

Combustion instability refers to pressure oscillations in the combustion chamber which, when encountered in a rocket engine, can cause an increase in heat transfer rates up to ten-fold resulting in engine destruction in the order of milliseconds.

There are three principal types of combustion instability [Refs. 1 and 2]: low, intermediate and high-frequency. Low frequency instability, or chugging, generally refers to oscillations up to approximately 100 hertz and is the result of coupling between the propellant feed system and the combustion process. Intermediate frequency instability, typically from 100 to 1000 hertz, is not fully understood but is thought to involve structural vibrations, feed system line resonances, vortex formation around sharp corners and high heat transfer rates. Pressure variations in this frequency range of instability, reach about five percent of the steady state chamber pressure and tend to be more of a nuisance than damaging to the engine. High frequency instabilities are associated with the acoustic modes of the combustion gases and chamber and are the result of disturbances which are driven by interaction

of the combustion process and the chamber geometry. Of these instabilities, the high frequency type is the most destructive, since it can result in pressure fluctuations exceeding 100 percent of the steady state chamber pressure.

The destructive nature of combustion instability in a rocket engine has resulted in a continuing effort toward its recognition and elimination.

Analytical models have served satisfactorily to indicate qualitative trends in the combustion process, but to date none have been able to give quantitative information which would enable the prediction of the onset of instability in a particular rocket motor. In fact, no general agreement has been reached concerning the specific cause(s) of combustion instabilities in liquid propellant rockets.

Droplet vaporization has generally been considered to be the rate controlling mechanism in many liquid propellant rocket combustors and some stability models have been based upon this phase of the overall combustion process. However, Strahle [Ref. 3] has suggested that while vaporization may be important, it cannot be the major supporting mechanism in combustion instability. Other data [Ref. 4] also appears to support this contention.

Vortex velocity refers to the circumferential or tangential velocity component within a cylindrical combustor. References 5, 6, 7, and other studies have shown that for a droplet vaporization limited system, the existence of a steady vortex velocity causes a dramatic change in the boundary

between stable and unstable combustion as shown in Fig. 1.

Reference 8 investigated the effect of tangential gas velocity as a means of controlling instability in a vaporization-limited combustion process. Both experimental and theoretical evidence are presented which indicate that a steady tangential velocity of low magnitude can readily excite the traveling (i.e., spinning transverse) mode of combustion instability in a planar two-dimensional combustor. The effect of injecting gaseous nitrogen into a two-dimensional liquid oxygen, gaseous hydrogen combustor was investigated in Refs. 9 and 10. These studies also found that transverse combustion instability was induced with tangential injection of nitrogen in the combustion chamber.

An initial investigation was conducted to study the effect of a steady vortex gas motion on combustion stability in a small uncooled three-dimensional research rocket motor [Ref. 11]. The specific objective of this investigation was to extend the work of Ref. 11 in order to determine the effects of magnitude and direction of vortex flow velocity on combustion instability in a rocket combustor of practical configuration.

II. GENERAL DISCUSSION OF THE PROBLEM

In general, Raleigh's criterion [Ref. 12] states that energy release in phase with a wave tends to drive the wave, and out of phase tends to dampen it. As mentioned above, several models, based on this criterion, have been proposed in the literature which can be used to predict the effect of a steady vortex gas flow on combustion instability.

Priem developed a model [Ref. 5] which considered the various physical processes (droplet atomization, vaporization, chemical reaction, injection, etc.,) in determining combustion instability. By assuming that the combustion rate was controlled by the slowest process, he was able to theoretically predict a minimum pressure disturbance that would be amplified by the combustion process.

The model employed was a two-dimensional annular section with small thickness and length. The transport equations utilized in Priem's mathematical model are developed in Ref. 13. Several plausible assumptions are made which simplify the model sufficiently for computer solution.

If droplet vaporization is considered to be rate limiting, an additional expression (model) is needed for this "energy source process." One vaporization model has been developed by Priem in Ref. 14. Models for other "rate limiting" steps are presented in Ref. 5. It is shown in Ref. 5 that vaporization and atomization are strongly dependent on tangential gas velocity. If injection or chemical kinetics were rate limiting,

the energy source process is shown to be independent of tangential gas velocity.

If it is assumed that vaporization is rate controlling, Priem's model, with no vortex flow, predicts stability boundaries as depicted in Fig. 1 from Ref. 5. To determine the significance of vortex flow in stability, calculations were performed using the vaporization model with a superimposed constant vortex velocity. Results are shown in Fig. 1 (from Ref. 5) where it is seen that even a small vortex velocity may effect the stability boundaries dramatically. Although experimental evidence supports the qualitative trends shown in Fig. 1 and 2, disturbance levels for onset of instability are found to be one to two orders of magnitude higher than predicted [Refs. 5, 6, 8, and 9].

Heidmann [Refs. 8 and 9) examined in some detail the effects of vortex flow in a two-dimensional circular liquid propellant combustor. These studies involved the injection of a tangential flow of an inert gas into a stable combustor. variable amounts of nitrogen were introduced in order to find the magnitude of V_θ required to produce instability. Heidmann found that the combustor, which was stable under conditions of no tangential gas flow, had definite stability boundaries dependent on magnitude of tangential gas velocity. He also found that combustor pressure oscillation amplitude was nearly linearly related to tangential gas velocity.

Heidman and Feiler [Ref. 8] proposed a model to explain the experimental and theoretical evidence that a tangential velocity did excite unstable burning. In this analytical

model it was assumed that the energy released during combustion depended on the vaporization rate which varied as $(\rho(t)|\Delta V(t)|)^{1/2}$ where $|\Delta V(t)|$ represents the net velocity difference between the liquid and gas. The extent of driving or damping the instability was determined by comparing the time variation of energy release with pressure variation and computing the net in phase or out of phase energy addition. This can be more readily visualized if the energy release is considered to vary as $|V|$-rather than $(\rho|\Delta V|)^{1/2}$. In this case the energy/pressure relationships can be explained in a simplified manner using Fig. 3 from Ref. 8. Figure 3(a) depicts the pressure variation with time for a traveling transverse wave with no steady tangential velocity component. Figure 3(b) shows a similar velocity variation. If the energy release is linearly related to the absolute velocity, the energy release can be depicted as in Fig. 3(b). It is evident that energy release is symmetric reaching a peak twice per cycle. Therefore, according to Raleigh's criteria, no energy is added tending either to drive or dampen the wave. If now a steady velocity in the plane of the wave is superimposed as shown in Fig. 3(c), the in-phase energy release increases at the expense of the out of phase energy release. Thus, the wave is driven. If the velocity had been biased in a direction opposite to the wave motion, the net energy addition would have been out of phase with the wave,, and the wave would have been dampened (Fig. 3(d)).

Nearly all the theoretical and experimental work on the effect of tangential gas velocity on combustion instability to this time has been two dimensional, and it was the purpose of this investigation to address the realistic problem of a three-dimensional combustor.

Kiels initial investigation [Ref. 11] attempted to show whether the evidence found for a two-dimensional combustor were also applicable to a three-dimensional rocket. He found that with a first tangential instability [Ref. 2] a moderate swirl in one direction tended to decrease the instability intensity whereas flow in the opposite direction tended to increase it. For small amounts of swirl, there was virtually no effect on instability strength (P_p) when the direction of swirl was changed, as was also the case for a high degree of swirl. However, instrumentation precluded determination of instability direction or accurate tangential velocity measurement.

III. EXPERIMENTAL APPROACH

A small uncooled rocket motor, described in Section IV, was used in conducting this investigation. Normal heptane and air were burned in the combustion chamber with mixture ratios from 12.1 to 15.2 at a nominal chamber pressure of 260 psia.

Air flow was divided into primary and secondary flow regimes in which secondary flow direction could be varied from the control console in a continuous test from clockwise to counterclockwise to straight. The manner of accomplishing this will be described later.

Secondary air mass flow rates were varied from 10 to 25 percent of the total air mass flow rate.

The motor was instrumentated with high frequency response pressure transducers in order to experimentally determine the effects of both the magnitude and direction of tangential gas velocity on the magnitude and direction of the combustion instability. Insert elements (Fig. 4), which directed secondary air flow, were varied in order to vary the magnitude of V_θ on different tests while maintaining fixed secondary mass flow rate.

A typical firing sequence will be discussed below. First, power was supplied to the igniter whereupon oxygen and methane were injected, mixed and ignited. Then secondary air was allowed to flow first in a clockwise or counterclockwise direction until a steady state flow rate was achieved. Primary

air flow was then initiated and after a few seconds fuel was injected at which point ignition took place. This configuration was allowed to burn for one to two seconds whereupon opposite swirl was selected followed by straight secondary air flow. Each flow regime was allowed to burn for one to two seconds. After a four to six second total burn, the fuel was cut off, followed by primary air, allowing the secondary air to continue to purge and cool the motor. Visual inspection of the motor was conducted before and after each run to ensure system components were intact and operational. Prior to each day's run instrumentation was allowed to warm up for two hours after which strain gage transducers were zeroed. All pressure transducers were calibrated (over full utilized span) with an Ampthor dead weight tester.

The magnitude and direction of the secondary air velocity could be estimated at the injector face from measured temperatures and mass flow rates. However, in the stability models it is not the inlet V_θ that is of importance, but rather the magnitude of V_θ of the total gas flow within the combustor. Determination of tangential velocity in the combustor during a hot firing presents some difficulties. A simplified approach was used in this study. Chamber gas velocity magnitude and direction were determined in cold flow tests and then scaled to the high temperature and pressure of actual test conditions in a method described in Section V. Although this procedure may not provide exact data for the hot firing condition, it does provide a means for accurately comparing the effects

of various magnitudes and directions of secondary air flow on the magnitude and direction of the velocity of the total gas flow.

Gas velocity was determined as described below. Air alone was allowed to flow within the combustor in both the primary and secondary regimes. A three hole pressure probe (shown in Fig. 5), was used to determine the flow direction at various radial positions. Once known, a velocity profile was determined, and a swirl component ascertained. These tests were conducted for various percentages of secondary air flow.

In order to predict the instability frequencies which might be encountered in the rocket engine, it is necessary to solve the wave equation which governs the flow field in an acoustic medium [Ref. 15]. Although the apriori application of the wave equation is questionable since a small disturbance assumption is made, it has been found empirically that the solution is valid even for oscillations of large amplitude [Ref. 16].

Solution of the wave equation yields frequencies that are a function of combustor radius, length, speed of sound in the medium and roots of a Bessel function of order N [Ref. 15]. For the combustor used in this investigation, the frequencies were determined to be as follows:

Instability Frequency in Hertz

Tangential	Radial	Longitudinal
1st mode 5280	11,000	3000
2nd mode 8750	21,000	6000

Identification of the type of instability could be determined not only from frequency data but also phase relationships and characteristic wave form. Mixed modes of instability can also exist but the predicted frequencies are far above any encountered in this investigation.

IV. DESCRIPTION OF APPARATUS

A. GENERAL

A small uncooled research rocket motor was constructed in the main by Kiel [Ref. 11] for the purpose of studying combustion instability in a biphase (liquid-gas) rocket combustion chamber. Both primary and secondary air flow metering devices were strengthened and redesigned to more accurately control and measure air flow rates. A new fuel injector (to be described later) was designed to provide a more uniform distribution and better atomization of fuel. It was felt that this would improve combustion efficiency (η_{c*}) in all operating regimes of burning. High frequency response pressure transducers were added in the combustion chamber to allow determination of instability type and direction of travel.

The rocket motor was mounted on a thrust stand located in the rocket test cell (Fig. 6). Rocket operation was directed from the control room from two control panels (Fig. 7a and b) overlooking the test cell. All data was recorded on instrumentation location in the control room (Fig. 8).

B. ROCKET MOTOR

The rocket motor is shown in Fig. 9. It is cylindrical in shape and made in several sections in order to allow for expansion and modifications. Constructed of stainless steel, the rocket motor had a contraction ratio of 9.4. The nozzle (Fig. 10) was bolted separately to the combustion chamber to

allow for future modifications in contraction ratio or nozzle geometry. Two static pressure taps were located in the plane of the igniter and just upstream of the nozzle. High frequency response pressure transducers (Fig. 11) were located at 90-degree intervals half way down the combustion chamber. Two Kistler (Model 615) and a photocon 352A pressure transducer were used in order to determine instability frequency, intensity and direction of travel. A photo port (Fig. 11) was available in the same plane as the high frequency pressure transducers for streak photography observation.

C. FUEL SUPPLY SYSTEM

A schematic of the fuel supply system is shown in Fig. 12 and photographed in Fig. 13. Fuel was supplied from a 20-gallon tank located in a remote cell. The fuel tank could be pressurized with nitrogen to 1000 psi. A liquid level indicator on the fuel tank, and one on the fuel control console (Fig. 14), indicated fuel quantity in percent of tank capacity. Fuel passed through a filter and an emergency shutoff valve activated from control console A (Fig. 7a). It then passed through a microporous filter and a Jamesbury on-off actuator controlled from console B (Fig. 7b). Locally manufactured cavitating venturis were employed to control the fuel flow rate. The venturis were calibrated by measuring flow rate as a function of upstream pressure. Upper limits of back pressure were established at which point cavitation ceased to occur. Fuel manifold pressures exceeding these limits would allow undesirable interaction of the feed system with the

combustion process and were to be avoided. Fuel then passed into the primary fuel injector manifold (Fig. 15) and then in order to pass through the labyrinth of primary and secondary air tubing, was routed to a secondary fuel manifold just upstream of the injector face. The centrally located fuel injector tube had sixteen circumferentially located holes drilled back toward the injector face at a 45-degree angle to provide for better atomization and mixing. In addition, four injectors elements were located at 90-degree intervals around the center injector element on a 3-1/2 inch diameter circle with single centered holes to ensure complete fuel distribution within the combustion chamber.

D. AIR SUPPLY SYSTEM

The air supply system is shown schematically in Fig. 12. Air was supplied by two banks of air tanks which were capable of supplying air pressure up to 3000 psi. The tanks were pressurized by an Ingersoll Rand 3500 psig capacity air compressor. Air pressure to the motor was regulated through a Grove powreactor dome controller. Air flow was divided into primary and secondary regimes where flow rates were measured using thin plate, sharp-edged orifices with 1/2d and 1d pressure taps, installed according to ASME specifications [Ref. 17]. Inlet air temperature was measured with a copper-constantan thermocouple located downstream of the orifice plates. Primary air was injected into the combustion chamber around the centrally located fuel injector [Fig. 18] and circumferentially located injector elements.

The center primary air inlet to the combustion chamber was configured such that the air flow was choked at the air manifold exit and then expanded to supersonic flow before entering the combustion chamber. Upon entering the combustion chamber, the flow shocked causing mixing of fuel and air at the injector face. The primary purpose of the airflow around the circumferentially located injectors was fuel atomization and its flow rate was dictated by the desired droplet size [Ref. 4]. Secondary air was directed into the secondary air manifold (shown schematically in Fig. 16 and pictorially in Fig. 17) where it was possible to select any combination of the three flow regimes: clockwise, counterclockwise, or straight. Each airflow regime was injected through four tubes spaced at 90-degree intervals around the injector face (Fig. 4). The straight-through mode passed directly into the combustor. The clockwise and counterclockwise flows were deflected at angles of 20, 30, or 40 degrees at the injector face by brass inserts held in place between the air orifice and air swirling plates (Fig. 4). The lower mass flow rate of secondary air was restricted by the ability of the flow orifice to properly meter the flow, and the upper limit by the amount of flow the secondary air solenoid valves would pass. It was found that low air mass flow rates produced an oscillation within the air feed system that could not be eliminated, thus restricting the allowable flow rates. Numerous attempts were made to isolate the problem, as it was not known initially whether the oscillations were due to instrumentation or due to the propellant supply system. Various air flow metering

orifices were used within the limitations prescribed by the ASME power test code [Ref. 17], but to no avail. Primary and secondary flow regimes were run individually with all instrumentation powered by separate power supplies with flow both directed to the rocket motor and fed directly to the atmosphere. This showed that the problem was not with the instrumentation or the downstream configuration. It was then concluded that the resonance was within the air feed system but efforts failed to eliminate it.

E. IGNITION

The ignition system is shown schematically in Fig. 19. The combustion mixture was ignited with a methane oxygen torch shown schematically in Fig. 20 and photographed in Fig. 21. Current was supplied to a matrix of four nichrome wires insulated by a mullite tube. Gaseous methane and oxygen were injected separately in concentric tubes around the mullite and mixed for a short distance prior to exposure to the spark. The igniter continued to burn until de-activated by a pressure sensing switch which shut off the methane, oxygen, and spark when the chamber pressure reached about 50 percent of its expected steady state value (Fig. 22).

F. INSTRUMENTATION

A summary of the instrumentation used is listed in Table I.

Primary and secondary air pressures and differential pressures were used with temperature readings to determine air flow rates. Air manifold pressure was required to determine

TABLE I

INSTRUMENTATION

Nominal Expected Reading	(PSIG) Pressure Measurement	Range (PSIG)	Manufacturer	Type	Max Linear Output (MV)
1400	Primary Air	0-2000	Teledyne 206-SA	*S	40
130	Primary ΔP	± 250	MB Electronics 520	S	$5x10^3$
1500	Secondary Air	0-2000	Teledyne 206-SA	S	40
50	Secondary ΔP	± 250	MP Electronics 520	S	$5X10^3$
750	Air Manifold	0-1000	Wiancko P2-1251	**B	$5x10^3$
950	Venturi	0-2000	Teledyne 206-SA	S	40
450	Fuel Manifold	0-1000	Teledyne 206-SA	S	40
270	Chamber-1	0-500	Teledyne 206-SA	S	40
270	Chamber-2	0-300	Wiancko P2-3086	B	$5x10^3$
270	High Freq. Chamber	0-1000	Photocon 352A		
270	High Freq. Chamber	0-1000	Kistler 615		
	High Freq. Chamber	0-1000	Kistler 615		

* S - Strain gage.

** B - Bourdon tube.

possible instability coupling with the air feed system. A steady air manifold pressure was necessary to ensure no coupling. Venturi pressure allowed for the determination of fuel flow rate and it was necessary that fuel manifold pressure be below a predetermined value to ensure that cavitation occurred in the venturi. Pressure readings from the low output strain gage transducers, were amplified by a factor of 100 and then fed into the control room where the signals were attenuated (Fig. 23) and recorded on a Honeywell 1508 Visicorder oscillo-graph (Fig. 25). Higher output signals were attenuated and recorded directly on the visicorder. High frequency response pressure transducers were utilized for instability detection within the combustion chamber. These transducers were located in the combustion chamber (Fig. 5) so as to give maximum information about the instability (direction of travel, type, strength, and frequency). The pressure variations from the photocon and Kistler transducers were recorded as an Ampex CP-100 magnetic tape recorder at high tape speed. The signals on the Ampex were then played back at slow speed onto the visicorder operating at its fastest speed (80-IPS). This procedure was necessary in order to view the three traces for the entire run simultaneously where frequency, phase and amplitude could be determined. The three signals were also photographed simultaneously on a three channel oscilloscope for phase relationship determination. The purpose for examining these traces on the oscilloscope was to ensure that no phase information was lost in

transferring the high frequency output from the tape to the visicorder. Examining these traces on the oscilloscope was accomplished on the first few runs only until it had been shown that no phase information had been lost.

V. RESULTS

A summary of the data obtained from this investigation is presented in Table II. Only data from successful firings where instrumentation and rocket motor were operating satisfactorily are reported. Run Numbers 1 through 6 employed 20-degree inserts and runs 7 through 17 employed 40-degree inserts.

Fuel flow, air flow rates and mixture ratio were computed using a simple data reduction program. Average chamber pressure between the two chamber pressure transducers is reported. It should be noted that disparity was never greater than 2 percent between these two transducers.

Difficulty was encountered in obtaining rocket ignition during tests at high secondary air flow rates with the 40-degree inserts. Altering the secondary air flow sequencing resulted in successful ignition. For this reason, sequencing was altered in almost all runs utilizing the 40-degree inserts. C* efficiency was calculated for each run using a theoretical c* predicted by using the computer program of Ref. 18.

Theoretical c* values are shown in Fig. 24. Instability frequency and direction (when determined) are also presented in Table II. In addition, calculated values of the tangential velocity at the wall and the ratio of injected tangential to injected total momentum are included.

TABLE II

DATA SUMMARY

Run	$\dot{M}_{fuel}$	$\dot{M}_{air}$	$\dot{M}_{sec\ air}$	$\dot{M}_{pri\ air}$	Mixture Ratio	Swirl	P_p	η_{c^*}	Insta-bility Frequency	Type	Direction	Fraction $\dot{M}_{sec}$	Chamber Press	V_θ	ϕ(%)
1	.187	2.71	.517	2.19	14.5	CW	.38/0	.94	9,450	2T	--	.19	262	84	1.45
	.187	2.72	.530	2.19	14.5	CCW	--	.93	--	--	--	.19	257	84	1.55
	.187	2.57	.389	2.18	13.7	ST	--	.80	--	--	--	.15	212	0	0.0
2	.189	2.99	.587	2.41	15.9	CW	.20/0	.96	9,450	2T	--	.20	289	80	1.57
	.189	2.99	.587	2.40	15.8	CCW	--	.95	--	--	--	.20	286	79	1.57
	.189	2.82	.436	2.38	15.0	ST	--	.85	--	--	--	.16	242	0	0.0
3	.175	2.68	.401	2.28	15.4	CW	.62	.95	9,920	2T	--	.15	257	67	.82
	.175	2.60	.397	2.21	14.9	CCW	.49	.95	9,920	2T	--	.15	252	70	.85
	.175	2.52	.324	2.19	14.4	ST	--	.85	--	--	--	.13	216	0	0.0
4	.175	2.55	.416	2.13	14.6	CW	.65	1.00	10,150	1R	NA	.16	260	82	1.00
	.175	2.53	.416	2.11	14.5	CCW	.61	1.02	10,150	1R	NA	.16	258	83	1.01
	.175	2.46	.347	2.11	14.0	ST	--	.86	--	--	--	.14	217	0	0.0
5	.177	2.27	.206	2.07	12.9	CW	.71	1.00	10,700	1R	NA	.09	238	48	0.26
	.177	2.26	.206	2.05	12.8	CCW	.68	1.03	10,500	1R	NA	.09	240	47	0.26
	.177	2.23	.191	2.04	12.6	ST	--	.83	--	--	--	.09	192	0	0.0
6	.173	2.15	.221	1.93	12.4	CW	.68	1.03	10,750	1R	NA	.10	228	55	0.35
	.173	2.13	.210	1.92	12.3	CCW	.63	1.04	10,750	1R	NA	.10	229	53	0.35
	.173	2.10	.191	1.91	12.1	ST	.45	1.03	10,550	1R	NA	.09	218	0	0.0

TABLE II (continued)

Run	$\dot{M}_{fuel}$	$\dot{M}_{air}$	$\dot{M}_{sec\ air}$	$\dot{M}_{pri\ air}$	Mixture Ratio	Swirl	P_p	η_{c*}	Instability Frequency	Type	Direction	Fraction $\dot{M}_{sec}$	Chamber Press	V_θ	ϕ(%)
7	.180	--	--	2.11	--	ST	--	--	--				--	0	0.0
	.180	2.72	.614	2.11	15.2	CCW	.60	1.01	9,280	1R	NA	.22	280	81	4.18
	.180	2.70	.592	2.11	15.1	CW	.70	.96	9,280	1R	NA	.22	260	79	3.91
8	.174	2.47	.318	2.15	14.2	CW	.69	1.06	9,950	1R	NA	.13	269	56	1.08
	.174	2.47	.318	2.15	14.2	CCW	.69	1.08	9,950	1R	NA	.13	272	56	1.08
	.174	2.47	.292	2.12	13.9	ST	.16	.86	6,080	1T	NA	.12	212	0	0.00
9	.175	2.36	.288	2.07	13.5	CCW	.69	1.07	10,250	1R	NA	.12	258	58	0.96
	.175	2.36	.288	2.09	13.5	CW	.75	1.07	10,150	1R	NA	.12	258	58	0.96
	.175	2.28	.251	2.03	13.1	ST	.18	.87	6,080	S1T	CCW	.11	203	0	0.0
10	.174	2.44	.435	2.00	14.0	CCW	.76	1.04	10,200	1R	NA	.18	259	77	2.33
	.174	2.43	.426	2.00	14.0	CW	.68	1.04	8,960/ 10,200	2T/ 1R	NA	.18	259	77	2.24
	.174	2.37	.366	2.00	13.6	ST	--	.83	--	--	--	.16	202	0	0.0
11	.169	2.43	.416	2.02	14.4	CCW	.71	1.03	9,380	2T	--	.17	257	73	2.11
	.169	2.43	.416	2.02	14.4	CW	.78	1.04	9,280	2T	--	.17	261	73	2.11
	.169	2.39	.372	2.02	14.2	ST	.70	1.04	10,400	1R	NA	.16	265	0	0.0
12	.172	2.45	.417	2.04	14.3	CCW	.74	1.04	9,450	2T	--	.17	263	74	2.07
	.172	2.45	.412	2.04	14.3	CW	.74	1.04	9,380	2T	--	.17	263	74	2.02
	.171	2.30	.354	1.95	13.5	ST	.13	.86	6,080	1T	NA	.15	202	0	0.0

TABLE II (continued)

Run	$\dot{M}_{fuel}$	$\dot{M}_{air}$	$\dot{M}_{sec}$ air	$\dot{M}_{pri}$ air	Mixture Ratio	Swirl	P_p	η_{c*}	Insta-bility Frequency	Type	Direction	Fraction $\dot{M}_{sec}$	Chamber Press	V_θ	ϕ(%)
13	.170	2.18	.210	1.97	12.8	CCW	.68	1.13	10,250	1R	NA	.10	252	50	.57
	.170	2.18	.210	1.97	12.8	CW	.23	1.02	4,650	S1T	CCW	.10	228	45	.57
	.169	2.15	.199	1.95	12.7	ST	--	.84	--	--	--	.09	178	0	0.0
14	.169	2.08	.205	1.88	12.3	CCW	--	.96	--	--	--	.10	202	44	.59
	.169	2.08	.205	1.89	12.3	CW	--	1.06	--	--	--	.10	224	48	.59
	.169	2.08	.205	1.89	12.3	ST	--	.84	--	--	--	.10	178	0	0.0
15	.173	2.56	.596	1.97	14.8	CCW	.197	.99	9,300	2T	--	.23	262	92	4.5
	.173	2.55	.585	1.97	14.8	CW	.394	1.01	6,080	1T	NA	.23	262	92	4.4
	.173	2.40	.431	1.97	13.9	ST	.426	.86	6,080	1T	NA	.18	211	0	0.0
16	.169	2.37	.384	1.97	14.0	CCW/ST	.75/0	1.10	4,640	1T	NA	.16	273	39	.27
	.169	2.37	.384	1.90	14.0	CW/ST	--	1.10	--	--	--	.16	273	39	.27
17	.166	2.29	.340	1.95	13.8	CCW/ST	.50/0	1.10	4,580	1T	NA	.15	262	36	.24
	.166	2.29	.340	1.95	13.8	CW/ST	--	1.10	--	--	--	.15	262	36	.24

One of the parameters of great importance in this analysis, was tangential gas velocity. Ideally it would be desirable to obtain this information from an actual firing. Due to the excessive gas temperatures within the combustion chamber, this was impossible. It was decided to obtain this information by scaling data obtained in a cold flow situation, with mass flow rates equivalent to those used in hot firings. This was accomplished as follows: A 3-hole pitot probe was rigged in the same plane as the high frequency pressure instrumentation. The radial position of the probe was varied in one-fourth inch increments across the combustion chamber to determine a flow direction and velocity profile. This data was obtained at 0, 10, and 22 percent secondary mass flow rates, with both the 20- and 40-degree inserts. Velocity values for secondary flow rate between these values were obtained by linear interpolation. In order to estimate the tangential gas velocity in the hot firings, the following analysis was employed. The mass flow rate during a hot firing was almost equivalent to that during a cold firing (neglecting the small mass flow rate of fuel)

$$(\rho AV)_{hot} = (\rho AV)_{cold} \tag{1}$$

$$\left(\frac{P}{RT}AV\right)_{hot} = \left(\frac{P}{RT}AV\right)_{cold} \tag{1a}$$

Pressure (P_{cold}), velocity (V_{cold}), and temperature (T_{cold}) were determined for each cold flow test. For actual rocket firings, pressure (P_{hot}) was measured and temperature (T_{hot}) was calculated using the experimental values of mixture ratio

and combustion efficiency. Assuming that $A_{hot} = A_{cold}$, Eq. 1a could then be used to calculate V_{hot}. Assuming that the velocity direction did not change between hot and cold flow tests, V_θ for the hot firings could be calculated. It was also assumed that the magnitude of any steady tangential gas velocity induced by the instability itself, was negligible with respect to the injection induced V_θ. It is recognized that although this analysis is not precise, it should give a good estimate of the velocity values in a hot run.

While obtaining the cold flow data, it was noticed that there existed regions of reverse flow close to the walls. Since it was not possible to obtain reliable velocity information very near the walls, it was decided to verify this using a tuft analysis. This analysis confirmed the reverse flow regimes and large amounts of recirculation in the chamber. It was hoped that the pitot probe results could be substantiated through conservation of momentum by comparing inlet momentum at the injector face with measured momentum at the plane of the pitot tube. The reverse flow near the wall precluded this analysis.

The momentum ratio of tangential momentum to the total momentum was computed at the injector face through knowledge of the primary and secondary flow rates, direction, temperature and pressure.

The results of the cold flow analysis are shown in Figs. 25 and 26. With the velocity magnitude and direction known, it is possible to determine the components of velocity in the

axial and tangential direction. These components are non-dimensionalized by V_{max} which occurred along the chamber centerline.

A typical visicorder output is shown in Fig. 27. This pressure-time trace was used to determine various output pressures and finally determine flow rates, and engine performance parameters. High frequency data output from the Kistler and Photocon transducers are shown in Fig. 28. The same output is shown in Fig. 29 with an expanded time scale. The output in Fig. 28 was used to determine the instability persistance, while the output in Fig. 29 was used to determine phase and amplitude information.

VI. DISCUSSION OF RESULTS

The instabilities encountered in this investigation were first radial, first tangential and second tangential. Type of instability was identified through phase and amplitude relationships obtained from the three transducer traces. Most of the instabilities encountered were first radial and thus not helpful in demonstrating the original objectives. Second tangential instabilities were more useful but determination of direction of travel was not possible. Spinning first tangential instabilities where direction of travel was readily identifiable would have been most conducive to studying the objectives of this study. These occurred only in runs 9 and 13. Run 13 was spontaneously unstable with a first radial instability during counterclockwise swirl operation. Upon selecting clockwise swirl, the instability switched to a spinning first tangential traveling in the opposite direction to the swirl. Instability amplitude during the counterclockwise phase was about 33 percent of that in the clockwise phase, which is consistent with Heidmann and Feilers hypothesis that energy added out of phase with a traveling wave tends to attenuate it and in phase tends to drive it. Attempts to repeat this test condition were unsuccessful.

The fuel injector used by Kiel and in his study was a single element injector which resulted in a fairly concentrated energy distribution within the combustion chamber. With this

fuel injector it was not possible to support combustion in the straight through mode of secondary air flow. A multi-element fuel injector (Fig. 18) was incorporated in the rocket motor for this investigation in an attempt to establish efficient combustion during all modes of operation. That is, it was desired to ensure equally complete combustion during burning with and without vortex flow. It was found that the straight through air flow mode of combustion could be sustained with the multi-element injector. However, the vortex flow continued to cause more efficient burning due to better droplet atomization and increased fuel residence time within the combustor. This resulted in combustion efficiencies with vortex flow of from .95 to 1.10 and from .80 to .87 with no vortex flow. This causes a slight degradation in the results since the effect of combustion efficiency and tangential gas velocity cannot be uncoupled in the results. There were two notable exceptions to the combustion efficiency norms. On run 6, a combustion efficiency of 1.01 was attained in the "no swirl" mode. This resulted from loss of the center fuel injector during mid-run. Loss of the center fuel element caused fuel and air to be premixed in the air manifold with subsequent increased combustion efficiency. Fuel injector loss was thought to have occurred during the straight through flow because a drop in air manifold pressure was observed at that time. Higher than usual η_{c*} in the straight mode also occurred on run 11, and its occurence remains unexplained.

Although a calculated η_{c*} above 1.00 is not theoretically possible, it is not unusual and is thought to be caused by an effective decrease in throat area due to boundary layer buildup and/or an effective throat reduction due to vortex flow.

Nearly all runs exhibited the tendency toward higher amplitudes of oscillatory pressure with more efficient combustion (η_{c*}) (see Fig. 30). Mixture ratio did not have a significant effect on the instability amplitude (see Fig. 31).

In general, the most unstable conditions occurred in the clockwise mode of operation as was found by Kiel who used the same basic combustor, but with a different injector.

In those tests where a first radial instability persisted in both the clockwise and counterclockwise mode, the instability amplitude was nearly constant. During the straight mode, the instability would disappear or switch stability modes to a first tangential instability with greatly reduced magnitude. This indicated that an energy coupling mechanism may exist due to tangential gas velocity. The tangential gas velocity appeared to drive the instability from a small amplitude first tangential mode to a large amplitude first radial mode.

In run 6 the injector failure during the straight mode allowed fuel and air to be premixed in the air manifold. The first radial instability which existed in the counterclockwise and clockwise modes of air flow persisted in the straight mode but with reduced amplitude.

In addition, inspection of Fig. 32 reveals that the magnitude of V_θ affected the mode of instability. In general, tangential velocities between 45 and 55 feet per second and 75 and 85 feet per second induced radial instabilities. Values of V_θ above, below and between these ranges induced first tangential or second tangential instabilities. This result is not predicted in the two-dimensional models.

On several runs (not reported) in which very high tangential velocities were present, it was not possible to ignite the motor due to excessive radial acceleration of the fuel-air mixture. Inspection of the rocket motor after these unsuccessful firings showed fuel stream traces almost circumferentially around the combustion chamber.

These results indicated that one of the primary effects of the tangential gas velocity was that it both increased the atomization and vaporization rate, which changes the axial distribution of available energy to a more concentrated profile and changes the radial distribution of available energy. At very high values of V_θ most of the fuel was concentrated near the wall which was conducive to tangential instabilities of stable operation if the motor could initially be ignited with this concentrated fuel distribution.

In addition to the effects of V_θ on the radial mode of instability, the magnitude and direction of V_θ may also affect tangential modes of instability. Most of the combustion instability models deal with tangential instabilities since radial instabilities are not permitted in a two-dimensional

model. Subsequent discussion will deal with the first tangential and second tangential experimental results of this investigation and the first tangential experimental results reported by Kiel [Ref. 11].

There were two runs where a second tangential instability persisted during both clockwise and counterclockwise modes of operation. In run 12, the instability strength remained constant whereas in run 3 the amplitude was reduced. It is felt that the amplitude reduction occurred due to energy being added out of phase with the instability direction of travel. However, the spin direction of the instability could not be ascertained on this run.

The weakest tangential instabilities tended to be the first tangential. The largest and smallest values of tangential velocity produced P_p values from zero to 0.4, whereas midrange values of V_θ produced stronger instabilities (see Fig. 32). Calculated tangential gas velocity near the well varied between 28 and 92 feet per second in this investigation. This suggests that V_θ limits may exist above and below which tangential velocity does not drive the tangential instability. This result was also evident in Kiel's investigation. Cold flow data from this investigation was used to calculate tangential gas velocity for his study. V_θ calculated in this manner ranged between 22 and 73 feet per second.

In the theoretical model employed by Feiler and Heidmann [Ref. 8] an upper limit of V_θ is predicted. The model predicts that, up to a point, increases in the in-phase energy release

(tangential gas velocity) results in stronger instabilities. Upon reaching a critical value of tangential velocity, further increases serve only to increase the average energy added to the system rather than the oscillating portion. High values of V_θ may also increase atomization and vaporization rates such that they may not be the rate limiting step(s) in the combustion process [Fig. 32].

It is notable that on several runs with high combustion efficiency (runs 14, 16, 17) and low tangential velocity, the combustor was stable. Although runs 16 and 17 were unstable initially during the transient, they recovered and remained stable thereafter. This stability occurred at the minimum tangential velocity of about 35 to 45 fps., which was almost precisely what Heidmann reported for the minimum V_θ required to induce a tangential instability in his tests with a two-dimensional combustor. The linear increase in oscillatory pressure amplitude with increased tangential velocity as found by Heidmann and Feiler [Ref. 5] in the 2-D combustor could not be verified in this investigation because the mode of stability changed from tangential to radial at intermediate values of V_θ.

In order to determine the magnitude of V_θ required to induce spontaneous tangential combustion instability in Priem's model, it is necessary to first calculate a value for the burning rate parameter $(\mathcal{L}=\frac{rm}{\mathcal{A}})$. Although the average burning rate of the propellant per inch (m) is not known for this combustor, it can be approximated. Since the combustion efficiency is generally about 100 percent, it might reasonably be

assumed that it takes the complete length of the combustion chamber to vaporize all the fuel. Using a combustion chamber length of 6-1/2 inches and assuming a constant value of "m" yields an "m" of .154. Then $\mathcal{L} = .033$. Using Priem's instability model results, as shown in Fig. 1 from Ref. 5, it is predicted that spontaneous instability would occur for $V_\theta \geq 20$ fps. This is in qualitative agreement with the results of this investigation, although several runs were also unstable in the straight mode of air flow. Both Priem's and Heidmann's analytical models and Heidmann's experimental results show a threshold value of V_θ above which the combustor is unstable and below which stable operation results. In general, the results of this investigation (Fig. 32) agree with this. However, it should be emphasized that neither Heidmann's experimental results nor Priem's analytical model predict an upper limit on tangential gas velocity as discussed above. In was found in this study that a limit value of V_θ did exist above which the rocket was stable.

Instead of discussing V_θ effects, it may be of equal importance to consider tangential momentum which has been shown to be of importance in solid propellant combustion instability [Ref. 19]. A plot of the injected tangential momentum vs. P_p is shown in Fig. 33. This figure indicates a limit on the sensitivity of instability strength to the ratio of tangential to total momentum as was also found for V_θ.

The quadrant configuration of the fuel injector resulted in an energy distribution that invited a second tangential and/or first radial instability. The unavailability of additional high frequency response transducers precluded determination as to whether a second tangential instability was spinning or stationary. For this reason, it was desired to create a spinning first tangential instability as this would lend to a more definitive analysis. To this end, the circumferentially located fuel injectors were sealed to closely duplicate a fuel injector used by Kiel [Ref. 11], whose investigation produced only first tangential instabilities. This effort was successful in producing a standing first tangential instability upon rocket ignition. However, the instability did not persist and was attenuated after about .1 sec. These runs had the smallest amount of tangential gas velocity (V_θ), which may well have been the threshold value above which an instability would have persisted as discussed above. Runs 16 and 17 represent those firings in which both straight and counterclockwise or straight and clockwise modes were fired simultaneously. Rocket ignition was not possible with only one mode selected as was also reported by Kiel.

Notable in this investigation is the closeness of frequency for the second tangential and first radial instabilities. This result is not predicted by existing models. Powell and Zinn [Ref. 20] have presented a solution to the nonlinear wave equation in three-dimensional space, using the method of Galerkin. Their analysis predicts the second

tangential and first radial modes of instability to oscillate at twice the frequency of the first tangential mode. The analysis further predicts first tangential instability frequency to be quite close to those predicted by linear theory. These results compare well with the results of this investigation.

In run 10 the mode of instability switched from second tangential to first radial in mid run during the clockwise mode of operation. This may also have occurred on other runs, but it was impossible to view the entire run so that detection of this phenomenon was not assured. This phenomenon of coupling between various instability modes is consistent with the results of Zinn and Powell [Ref. 20].

CONCLUSIONS

It was found in this investigation that for a three-dimensional liquid-gas combustor, tangential momentum and/or gas velocity had a significant effect of combustion instability.

First radial instabilities were unaffected by direction of tangential gas velocity but occurred only at specific values of V_θ. This suggests that the tangential gas velocity (momentum) can affect the first radial instability by changing the radial energy distribution within the combustor.

When second tangential instabilities were encountered during operation with swirl in a particular direction, changing the direction of swirl caused the instability to be attenuated or driven.

When first tangential instabilities existed, instability direction could be determined. When instability direction was opposite to the swirl a dramatic reduction in instability strength resulted.

Upper and lower limiting values of V_θ were found above and below which the combustor was stable. The lower limit was found to be in qualitative agreement with the experimental results of other investigators using different combustor configurations. In addition, this lower limit was also in qualitative agreement with the analytical models of Feiler and Heidmann [Ref. 8] and Priem [Ref. 5].

Coupling between the various modes of combustion instability (first radial, first tangential and second tangential) was also observed in agreement with the work of Zinn and Powell [Ref. 20].

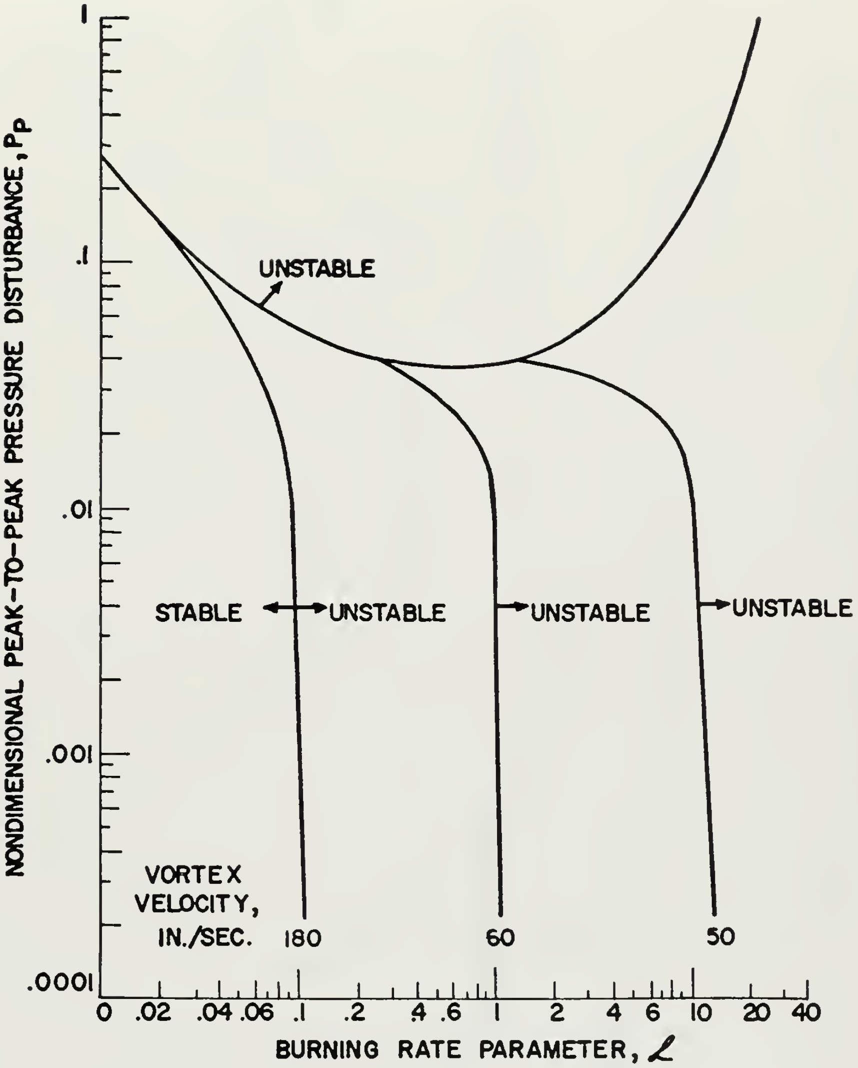

FIGURE 1 .INSTABILITY BOUNDARIES FOR VAPORIZATION MODEL WITH VORTEX FLOW [REF. 5]

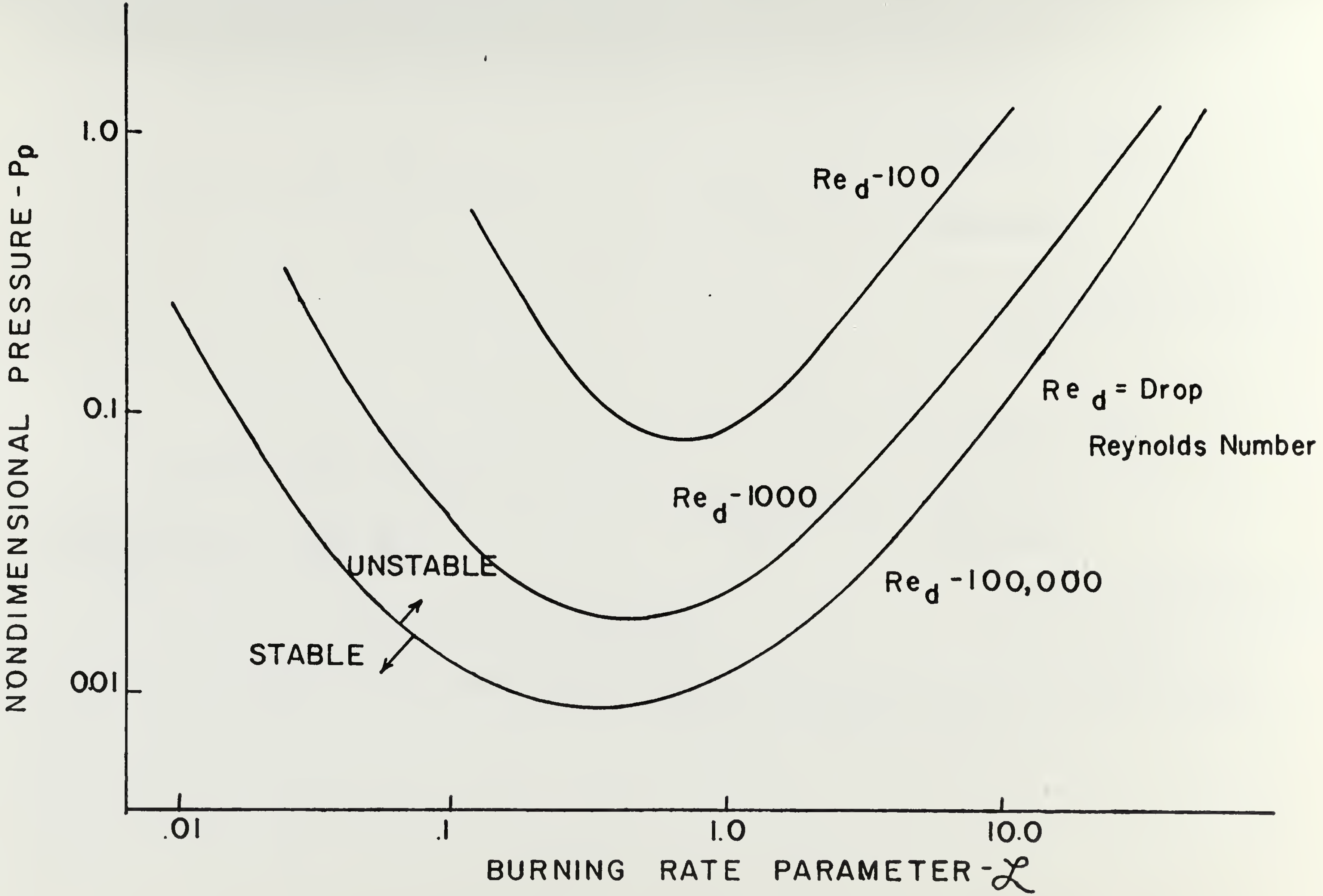

FIGURE 2. INSTABILITY BOUNDARIES (REF. 21)

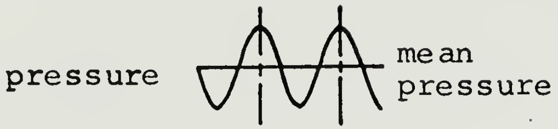

(a) pressure oscillation

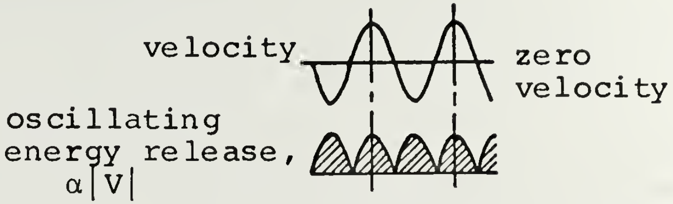

(b) velocity oscillation for traveling wave with no steady flow in plane of wave.

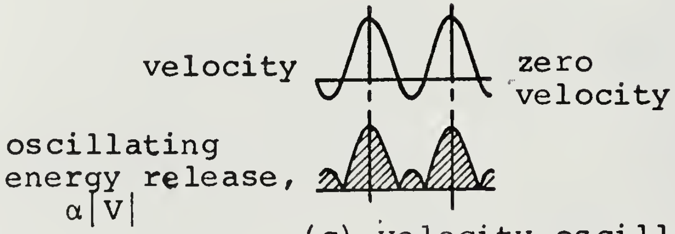

(c) velocity oscillation for traveling wave with steady flow in direction of wave.

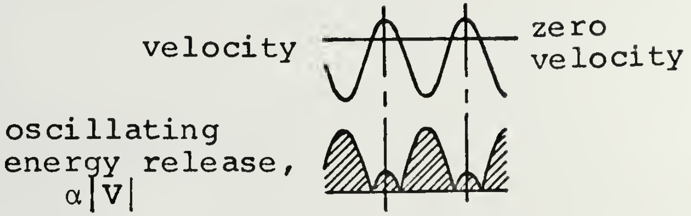

(d) velocity oscillation for traveling wave with steady flow in opposite direction of wave.

FIGURE 3. PHASE RELATIONS FOR SPINNING TRANSVERSE WAVES (FROM REF 8)

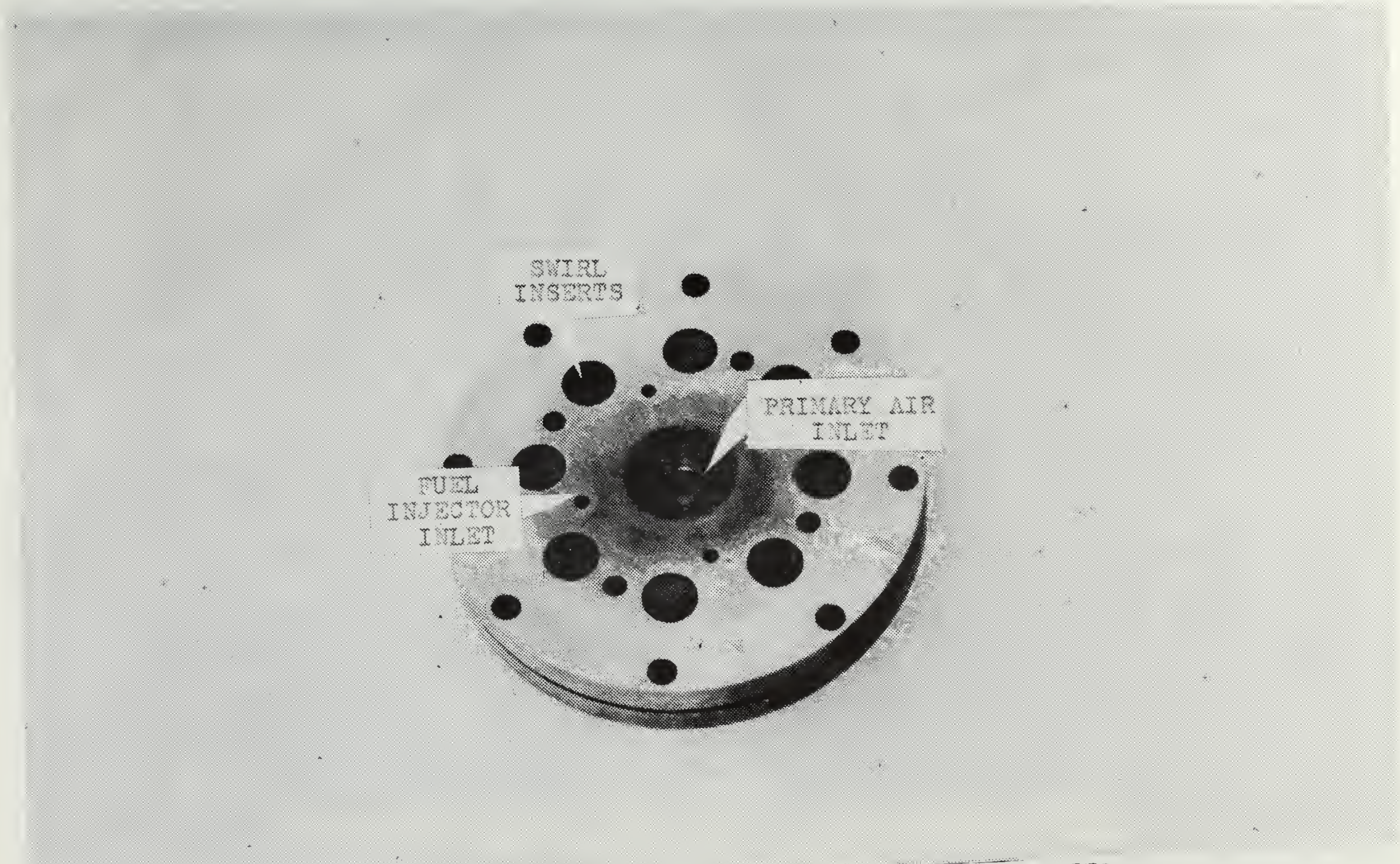

FIGURE 4. AIR ORIFICE AND AIR SWIRLING PLATES

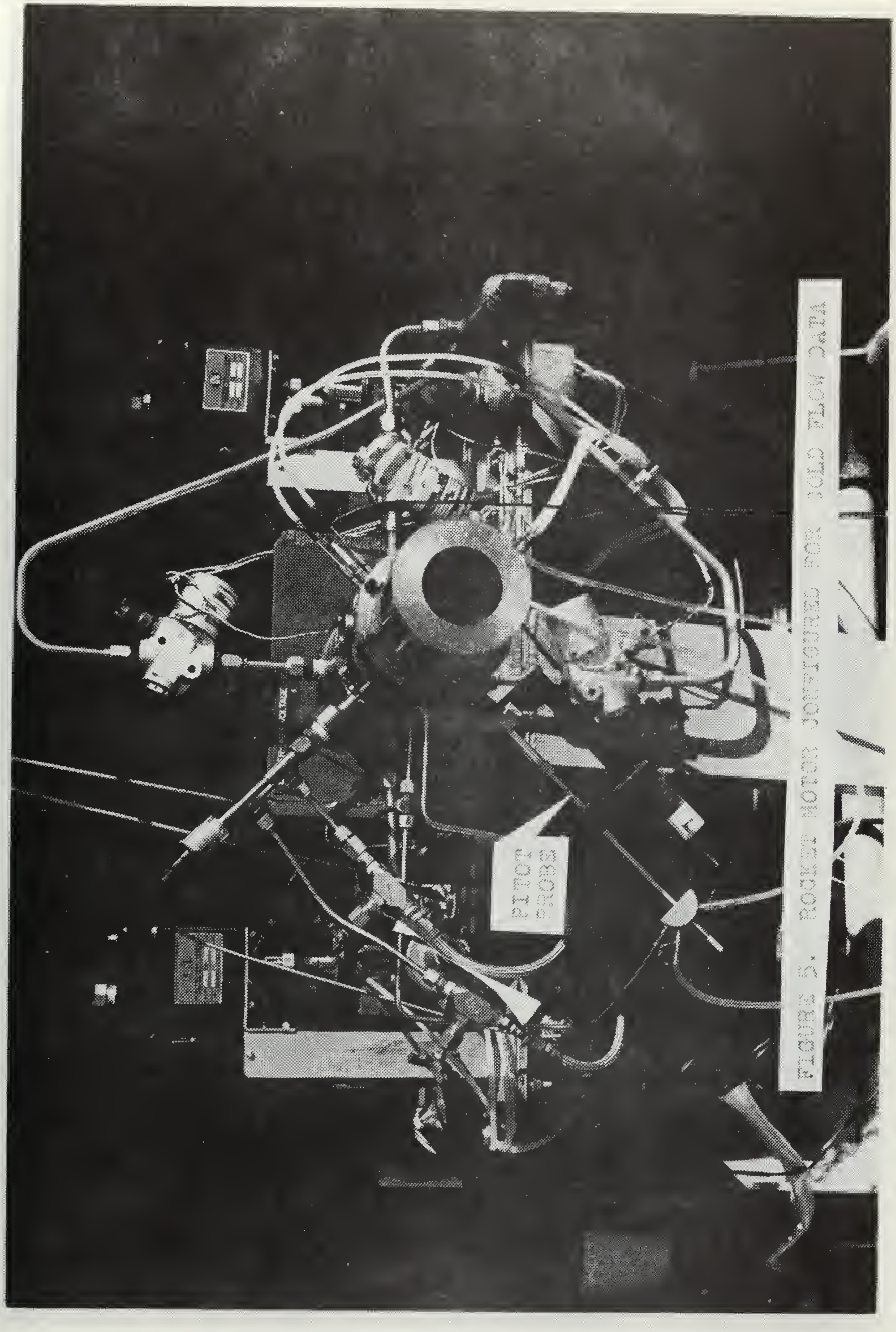

FIGURE 5. ROCKET MOTOR CONFIGURED FOR COLD FLOW DATA

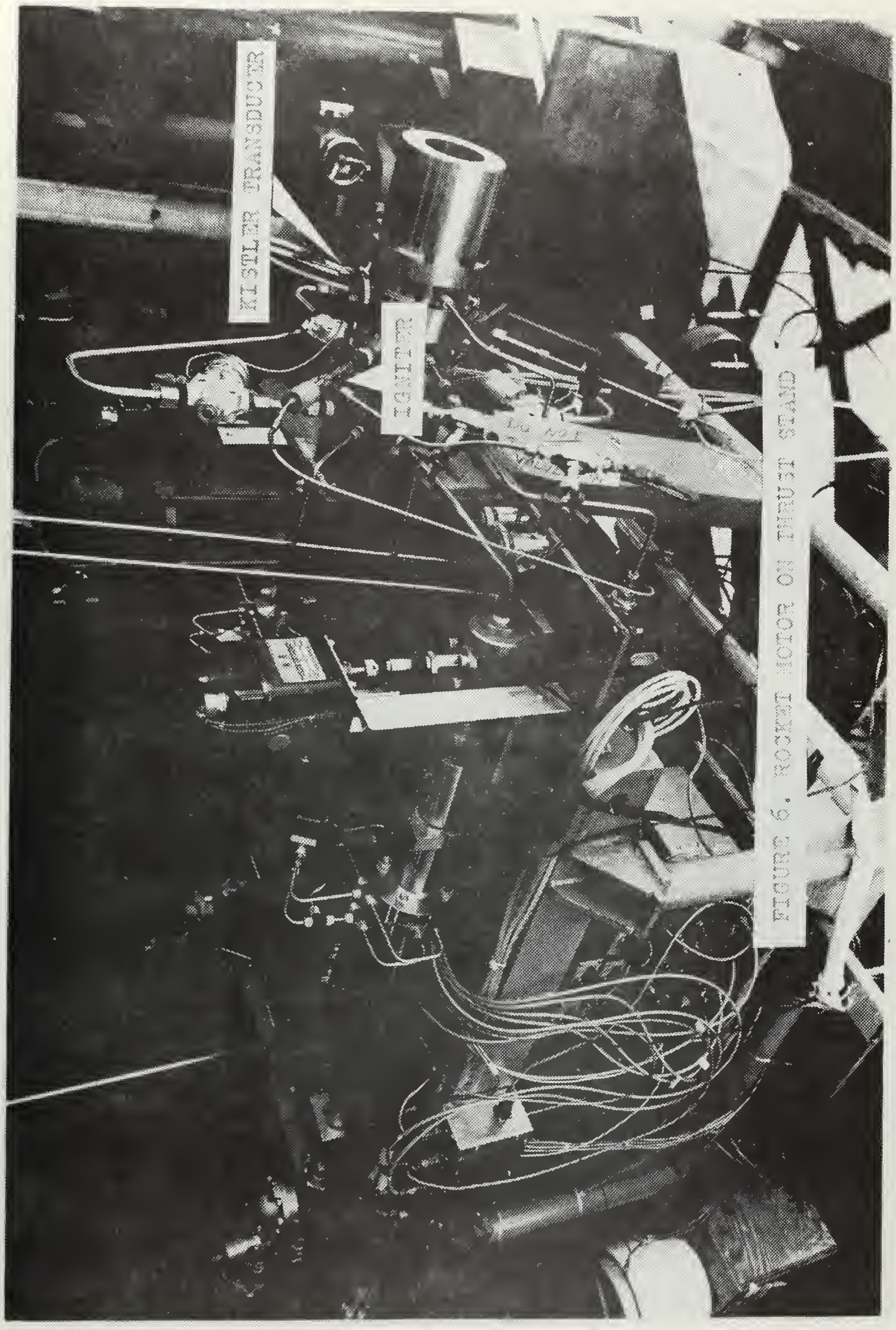

FIGURE 6. ROCKET MOTOR ON THRUST STAND

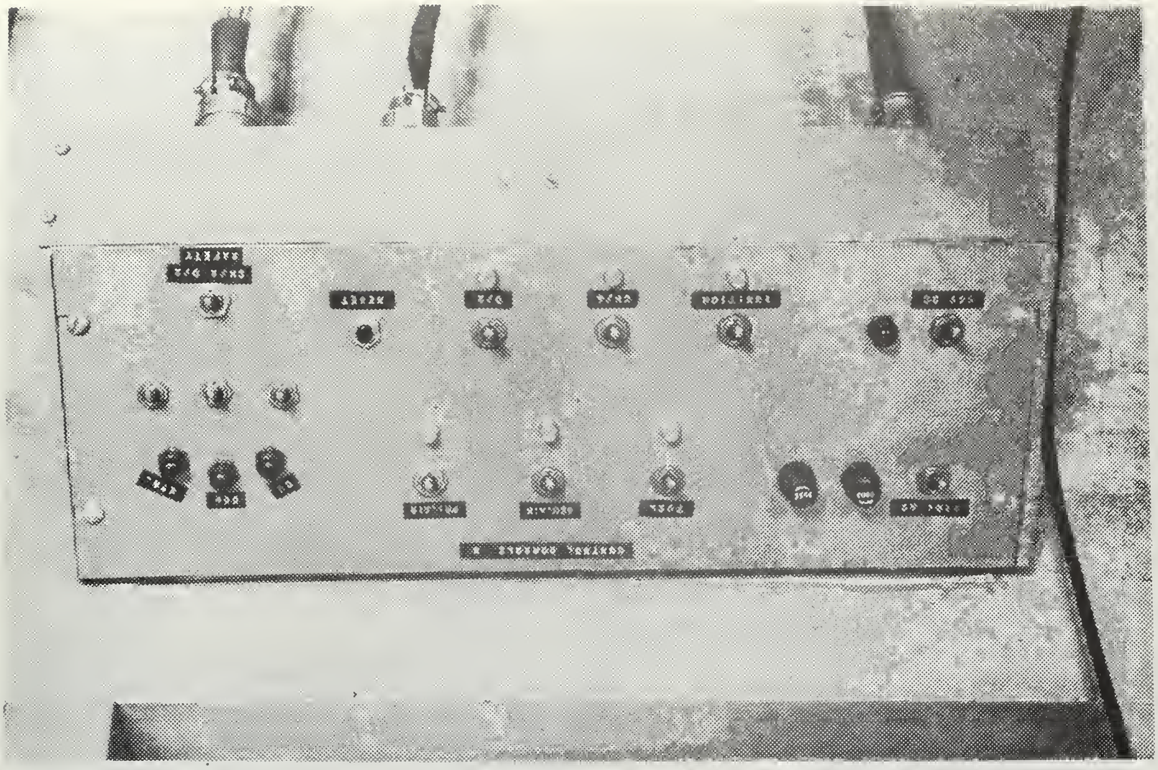

Figure 7a. Control Console A

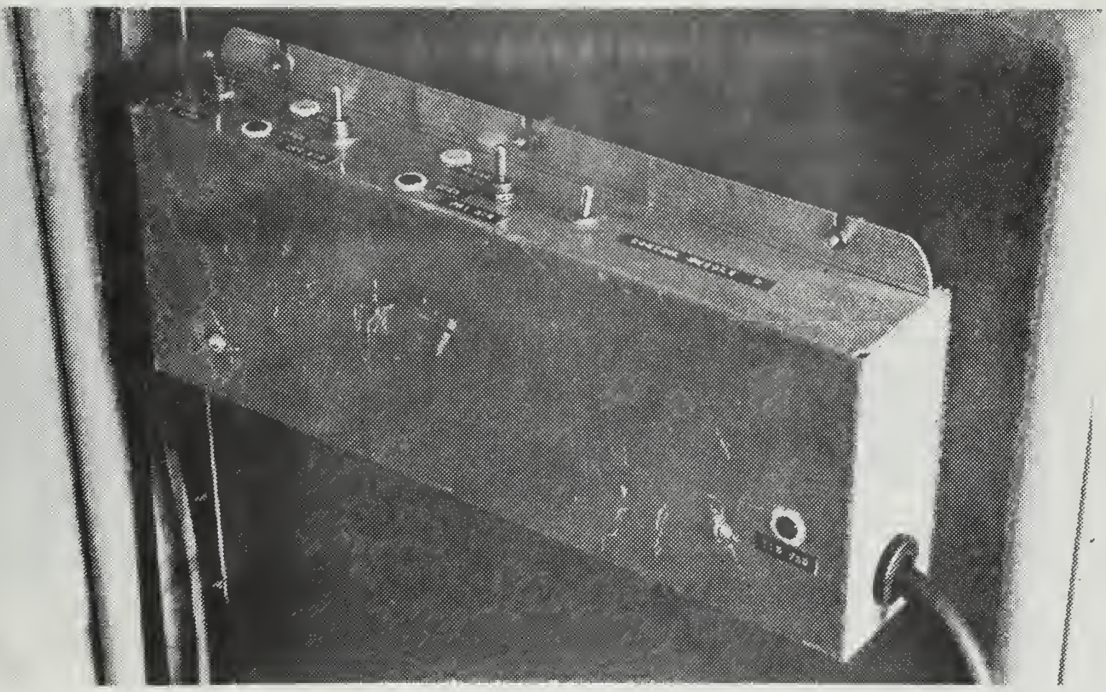

Figure 7b. Control Console B

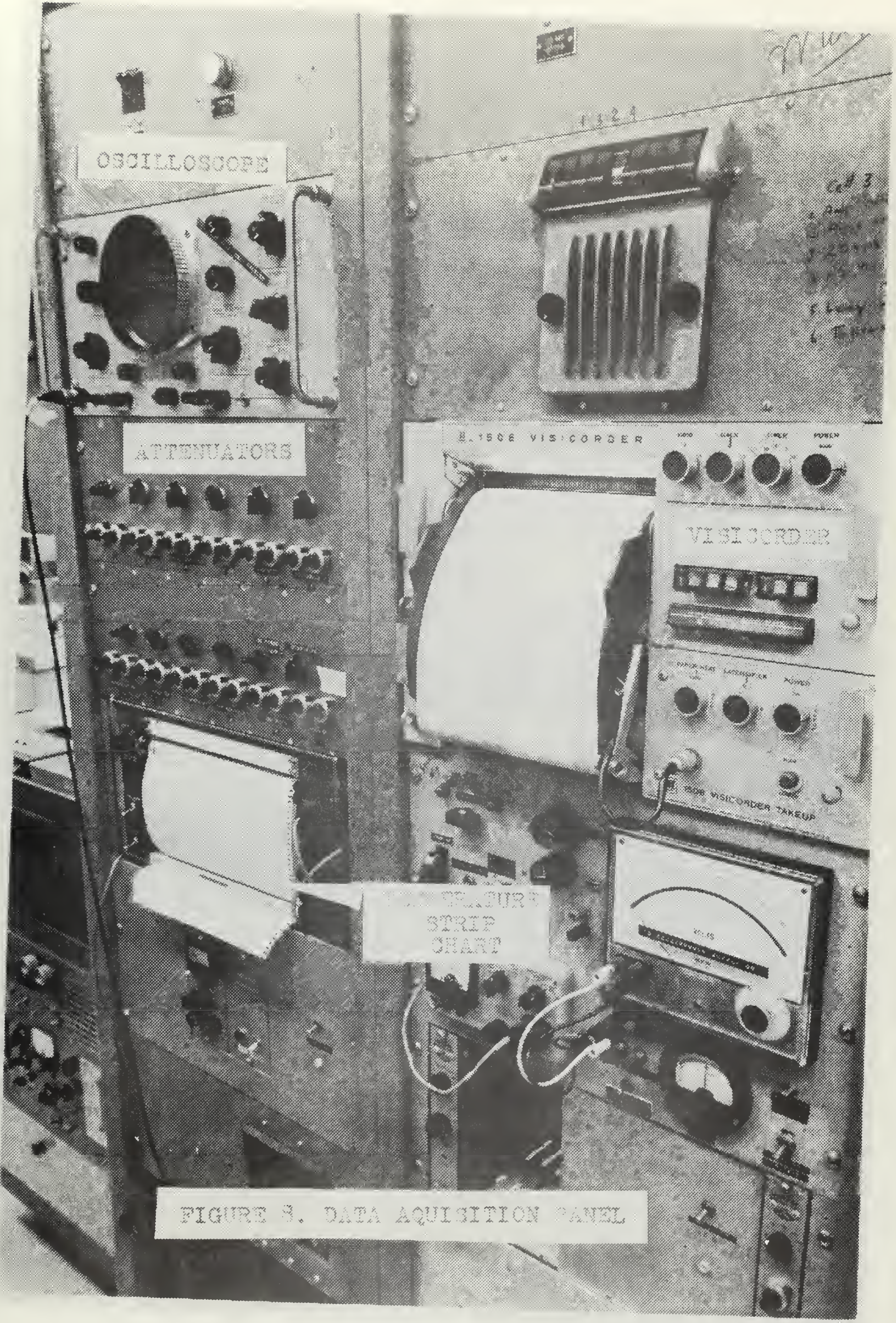

FIGURE 8. DATA AQUISITION PANEL

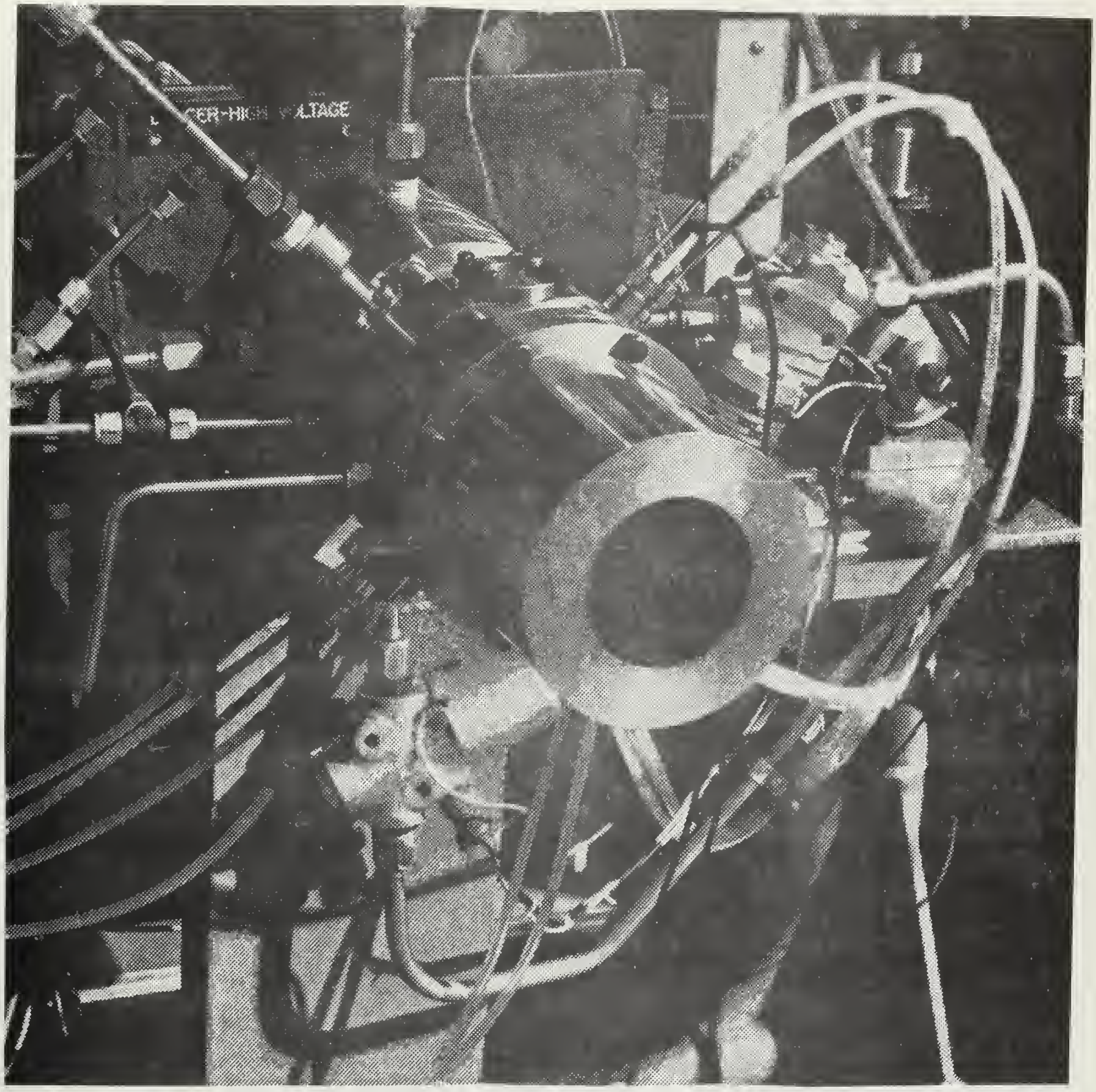

Figure 9. Rocket Motor

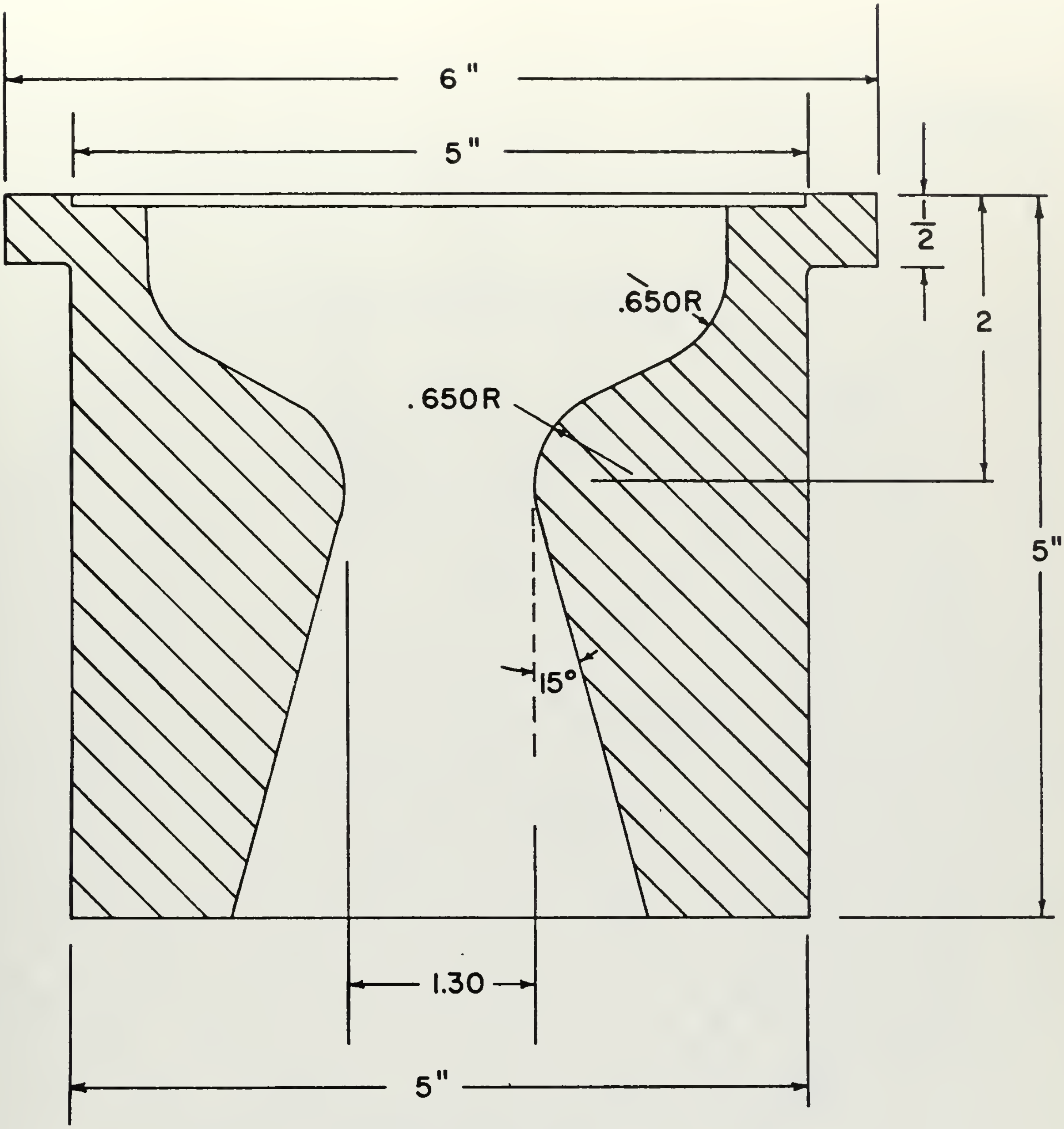

FIGURE 10

NOZZLE

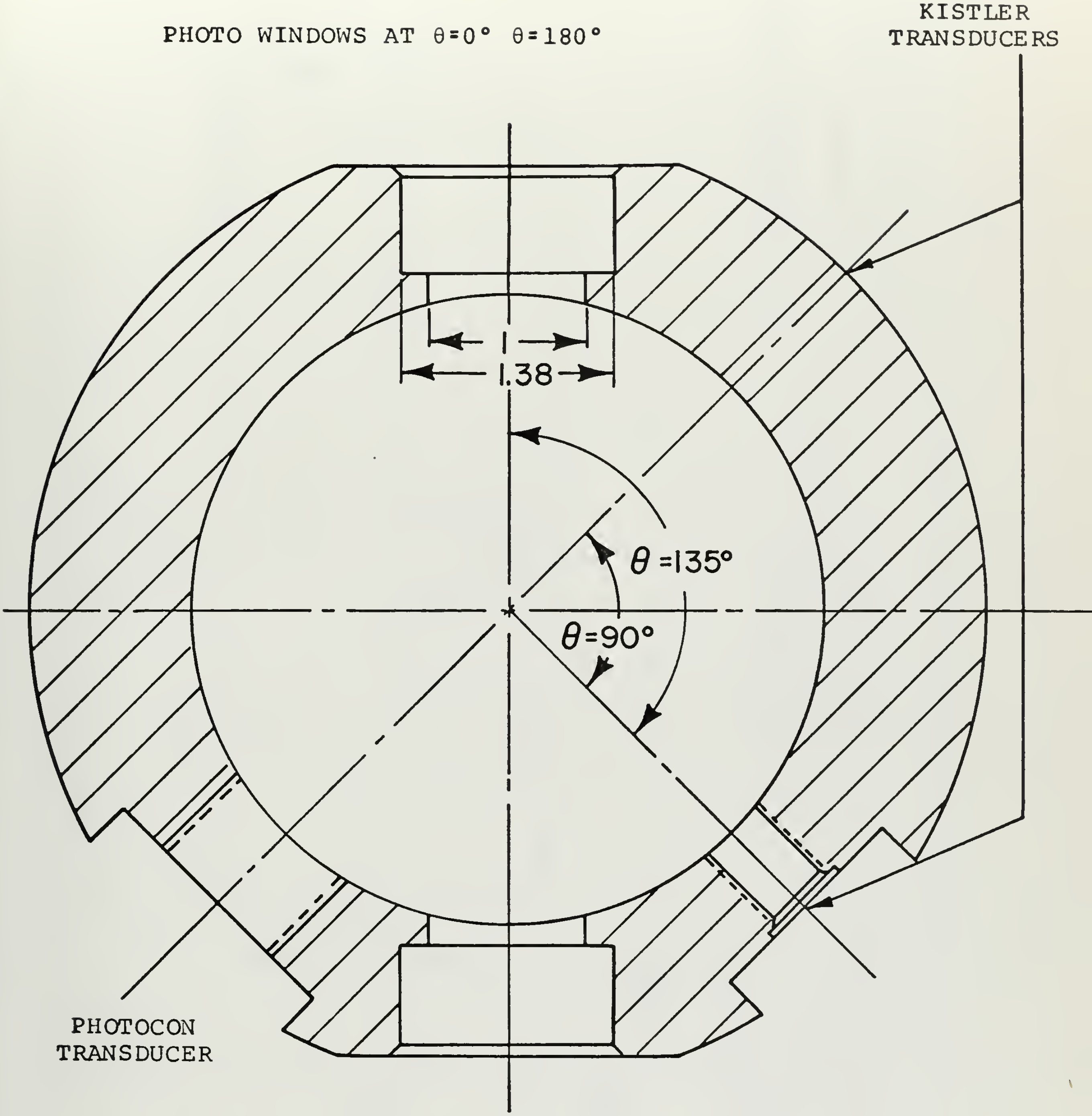

FIGURE II. HIGH FREQUENCY INSTRUMENTATION AND PHOTOGRAPHIC WINDOWS

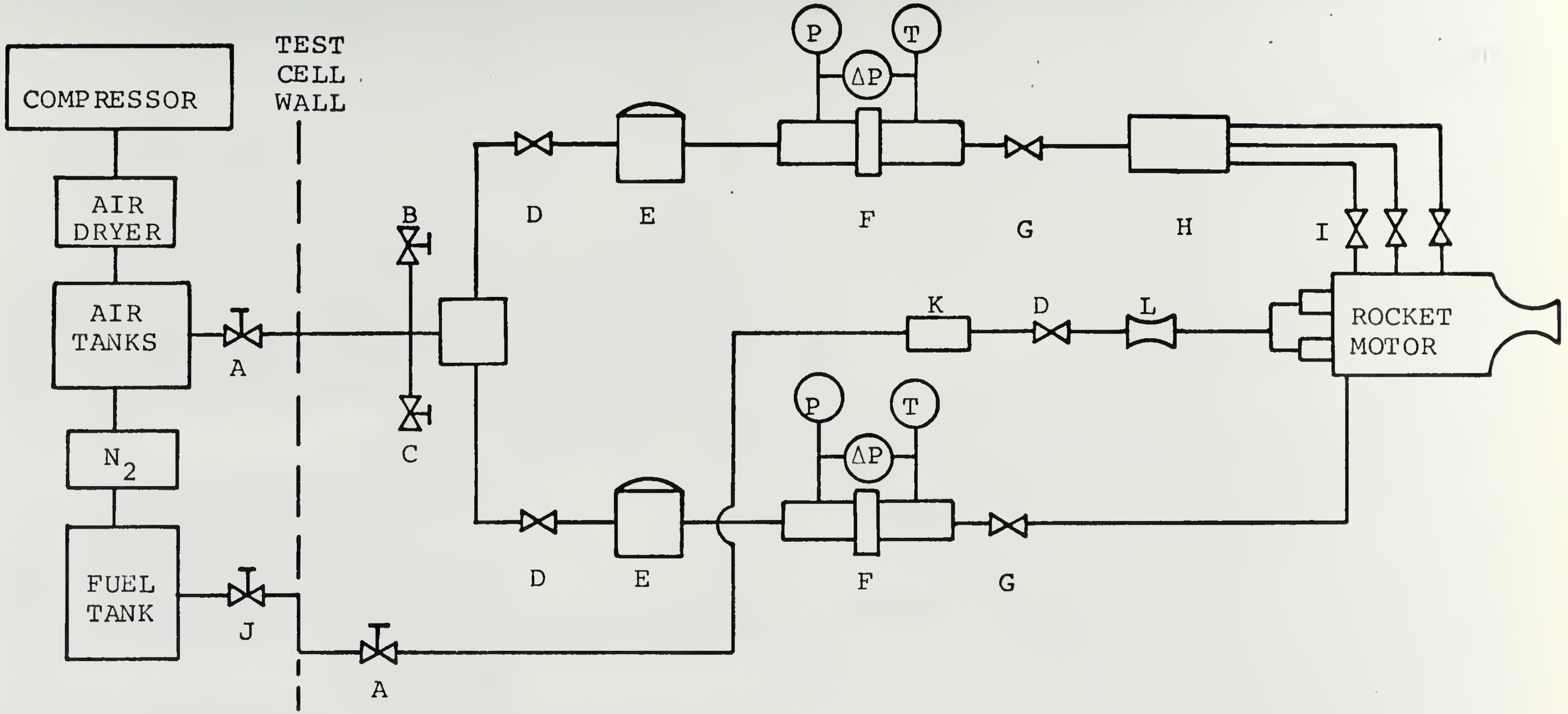

A - SHUTOFF VALVE (M)
B - AIR VENT (R)
C - AIR VENT (M)
D - ON-OFF ACTUATOR
E - DOME LOADED
PRESSURE REGULATOR

F - ORIFICE
G - FLOW REGULATOR
H - SECONDARY AIR MANIFOLD
I - SOLENOID VALVES
J - SHUTOFF VALVE (R)
K - FUEL FILTER

L - CAVITATING VENTURI
M - AIR FILTER

(R) remote actuation

(M) manual operation

Figure 12. Propellant Supply System

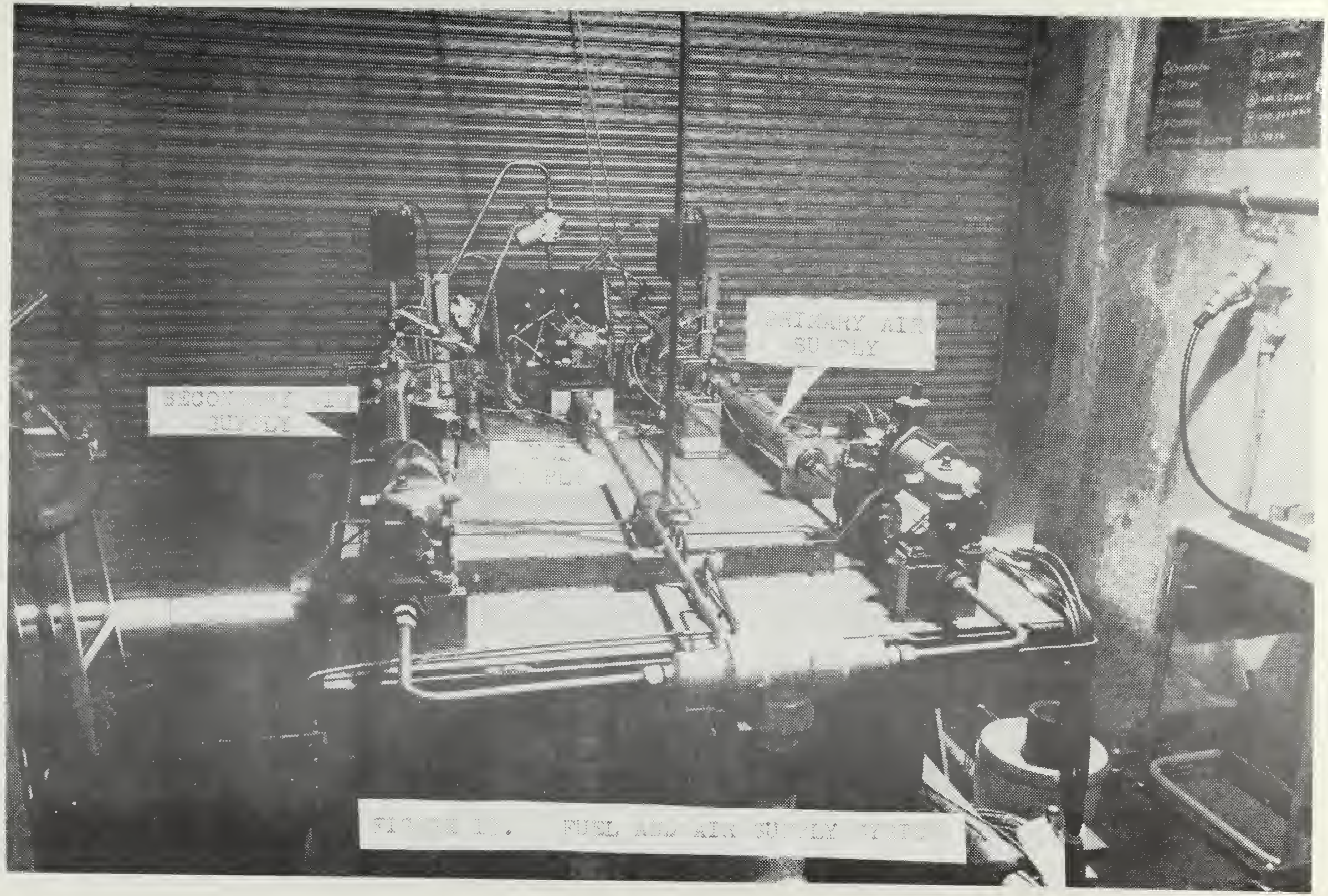

FIGURE 1[illegible]. FUEL AND AIR SUPPLY SYSTEM

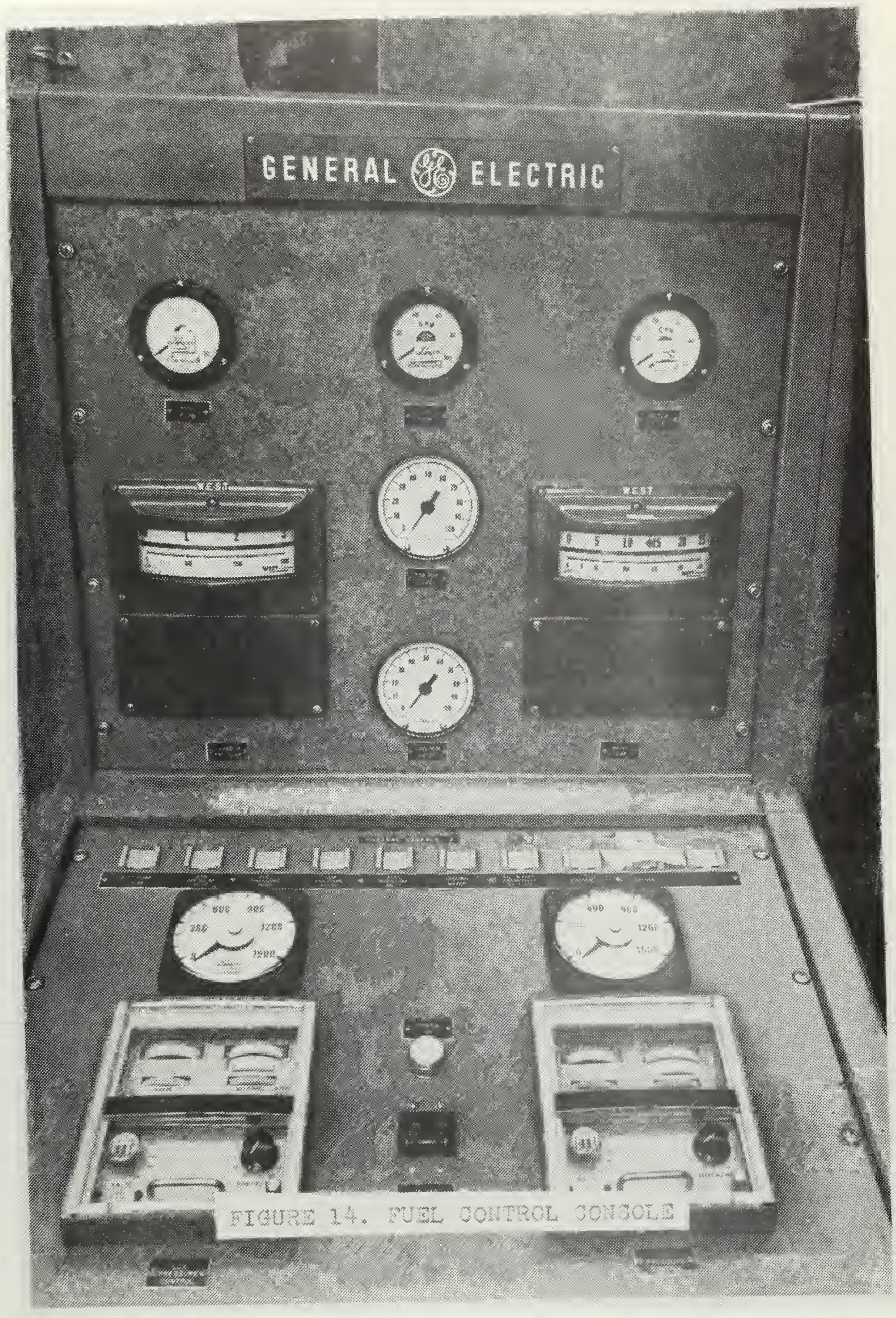

FIGURE 14. FUEL CONTROL CONSOLE

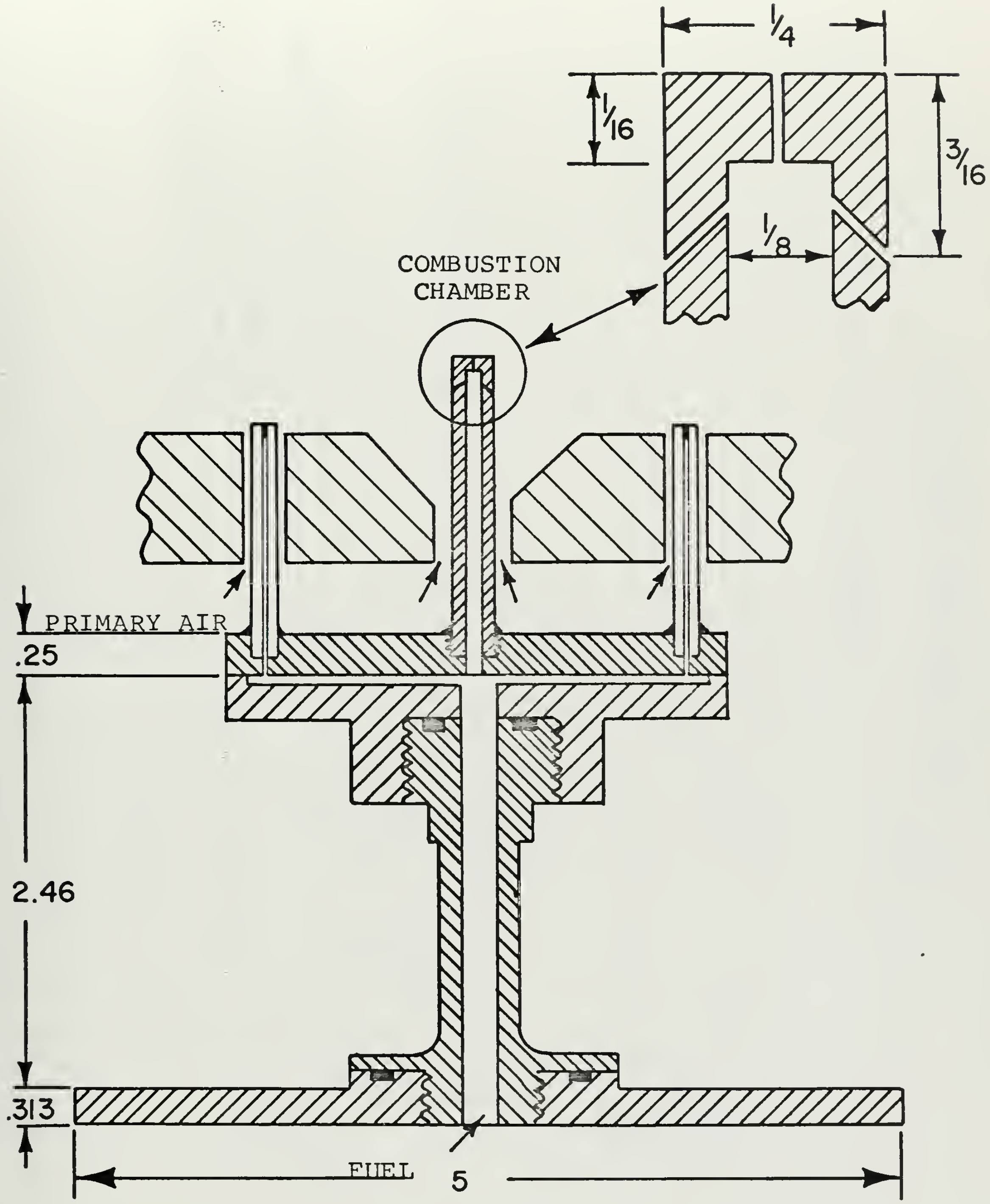

FIGURE 15. FUEL INJECTOR

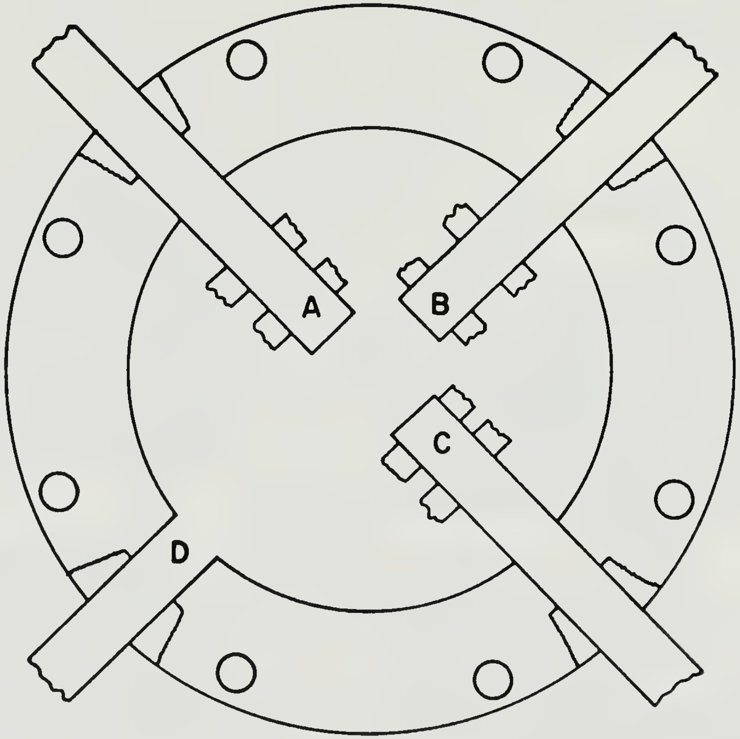

A-Secondary Air, Clockwise Swirl*

B-Secondary Air, No Swirl

C-Secondary Air, Counterclockwise Swirl*

D-Primary Air

* As Viewed From Injector

FIGURE 16

AIR INJECTOR MANIFOLD

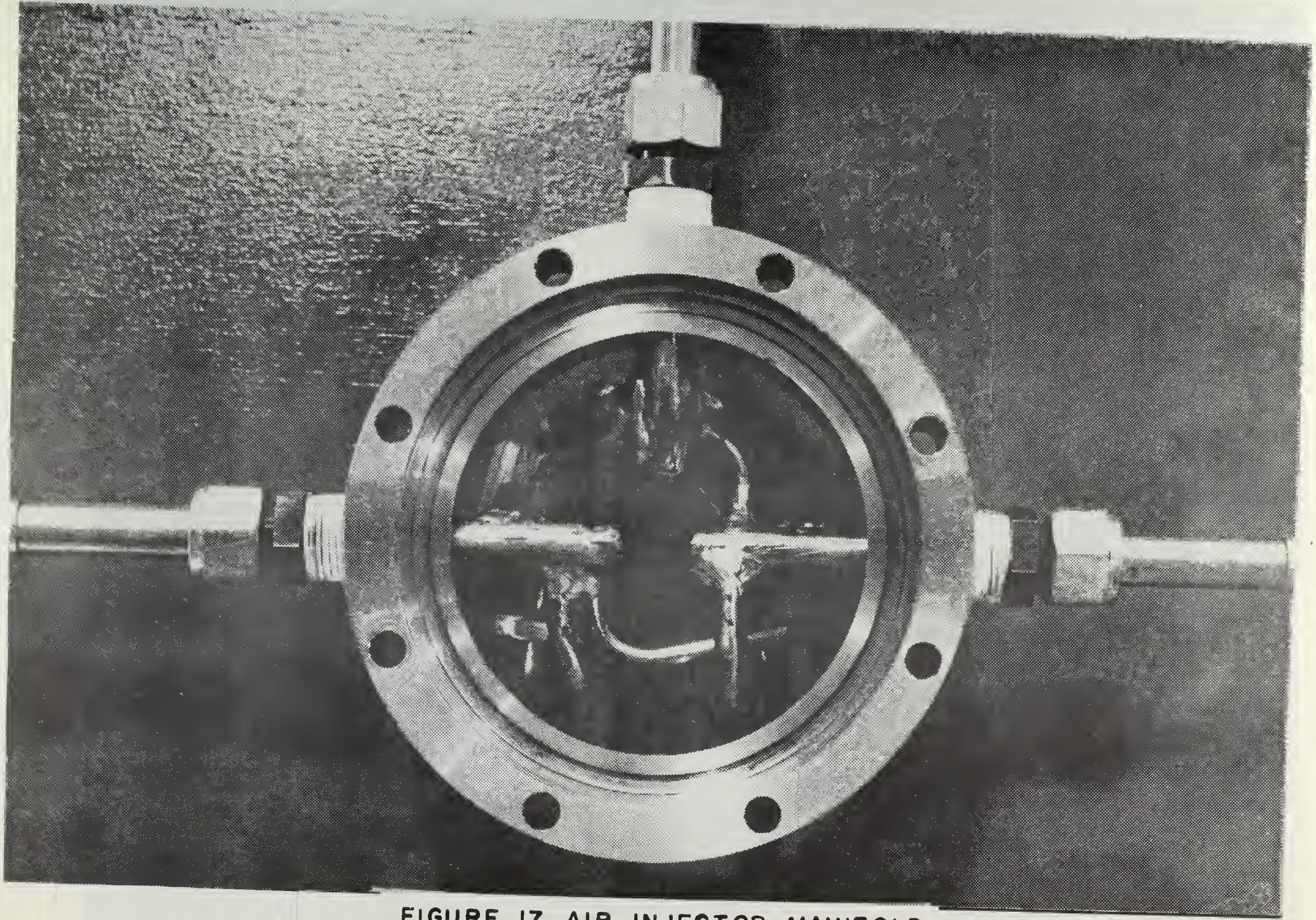

FIGURE 17. AIR INJECTOR MANIFOLD

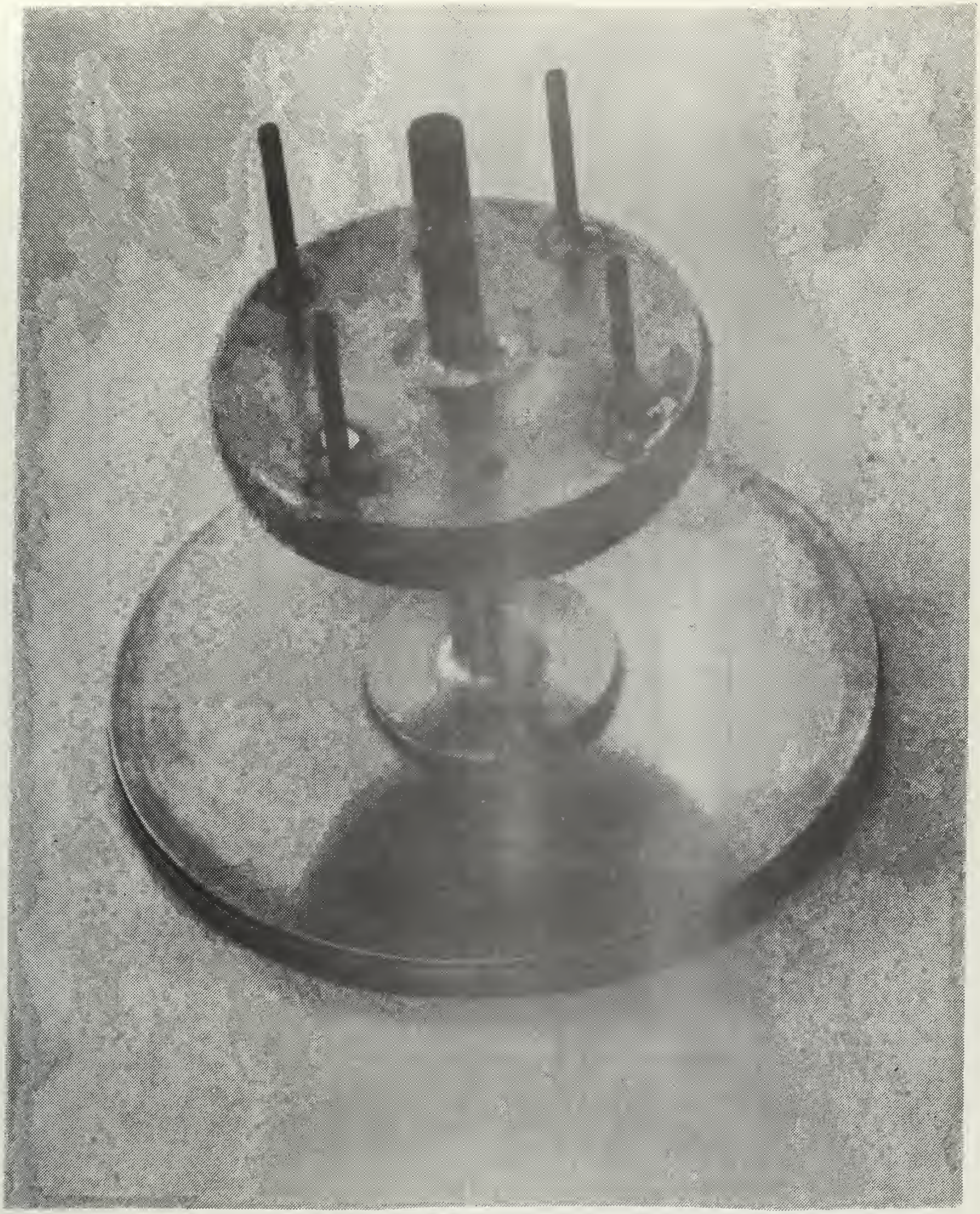

Figure 18. Fuel Injector

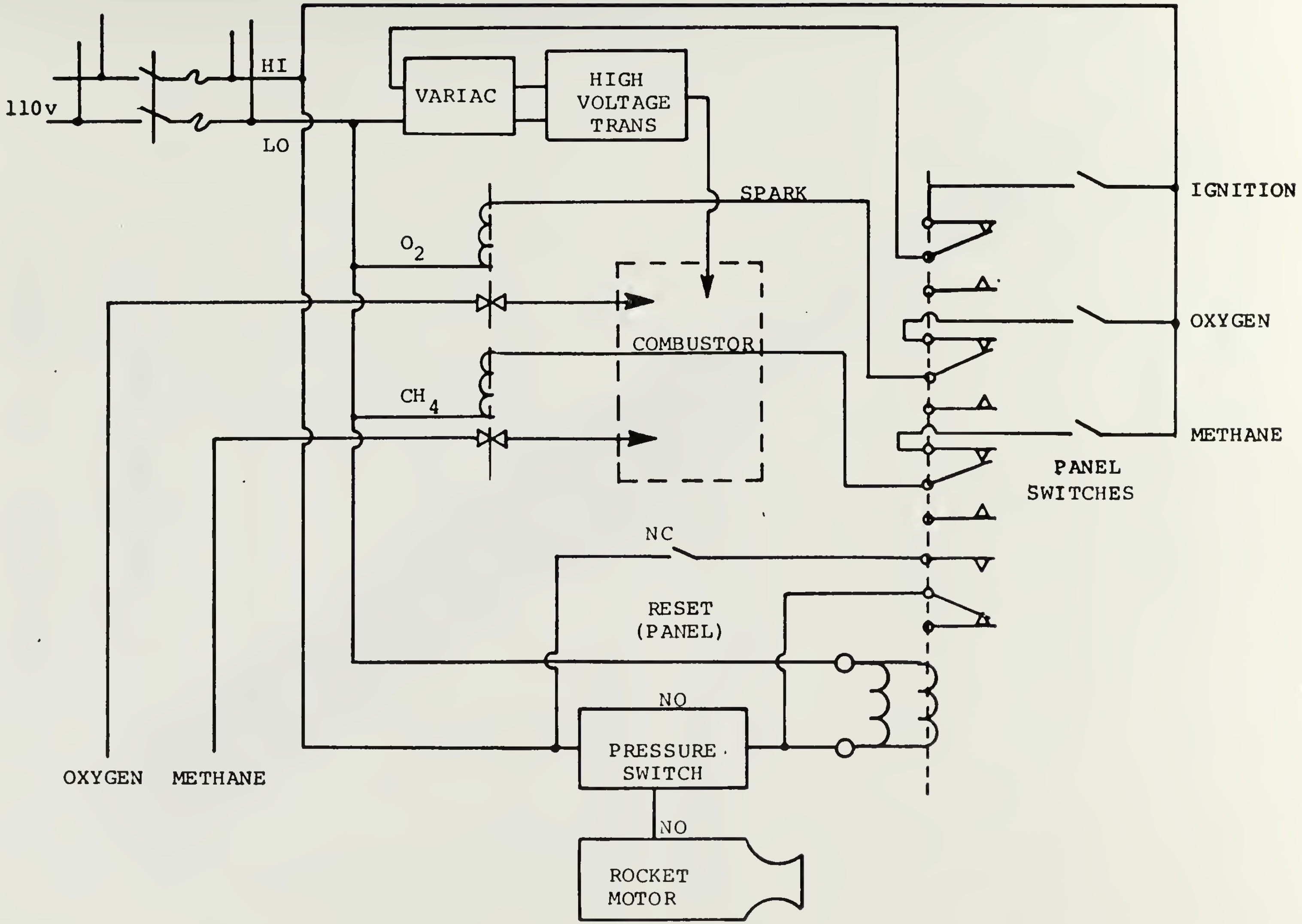

FIGURE 19. IGNITION SYSTEM

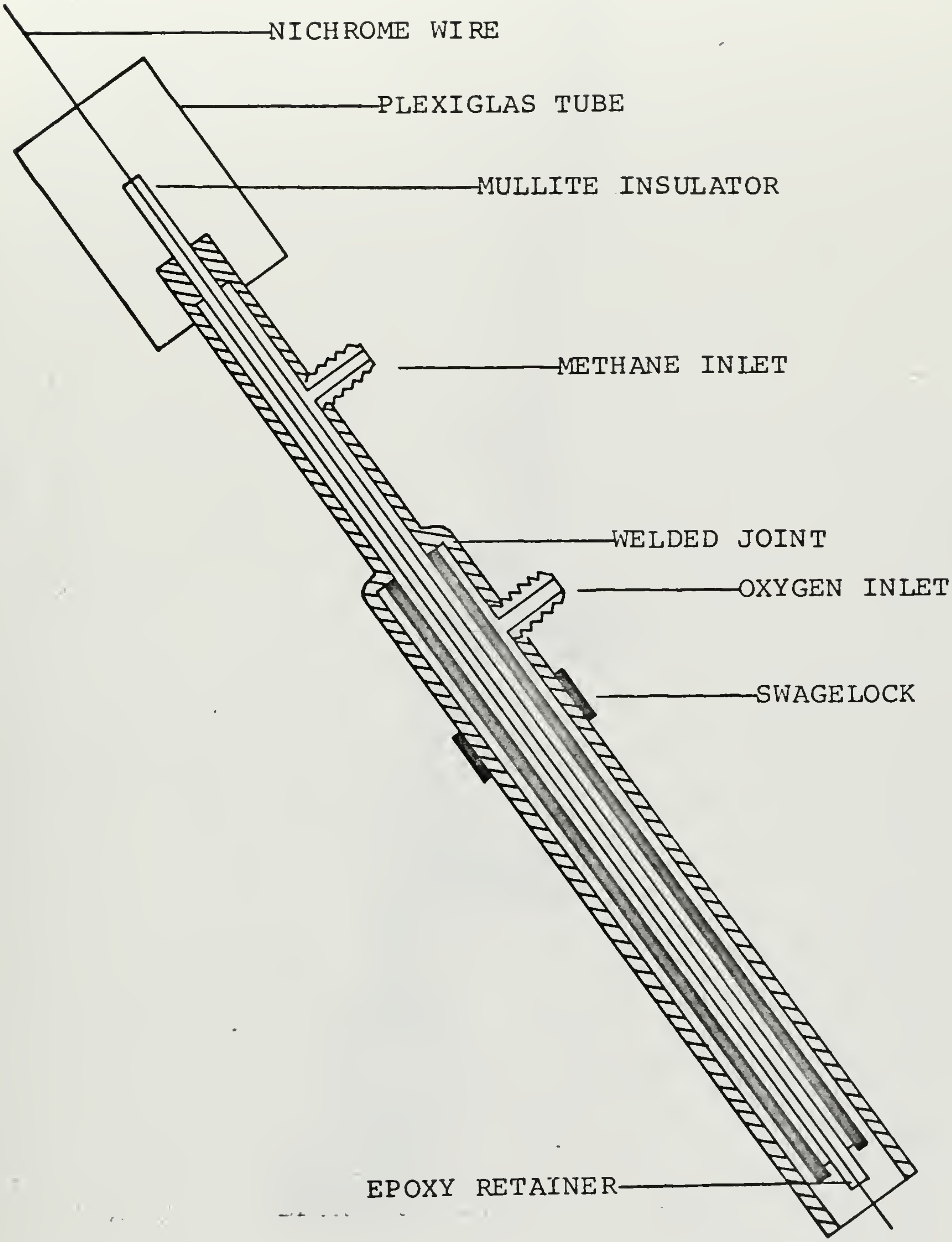

FIGURE 20. IGNITER

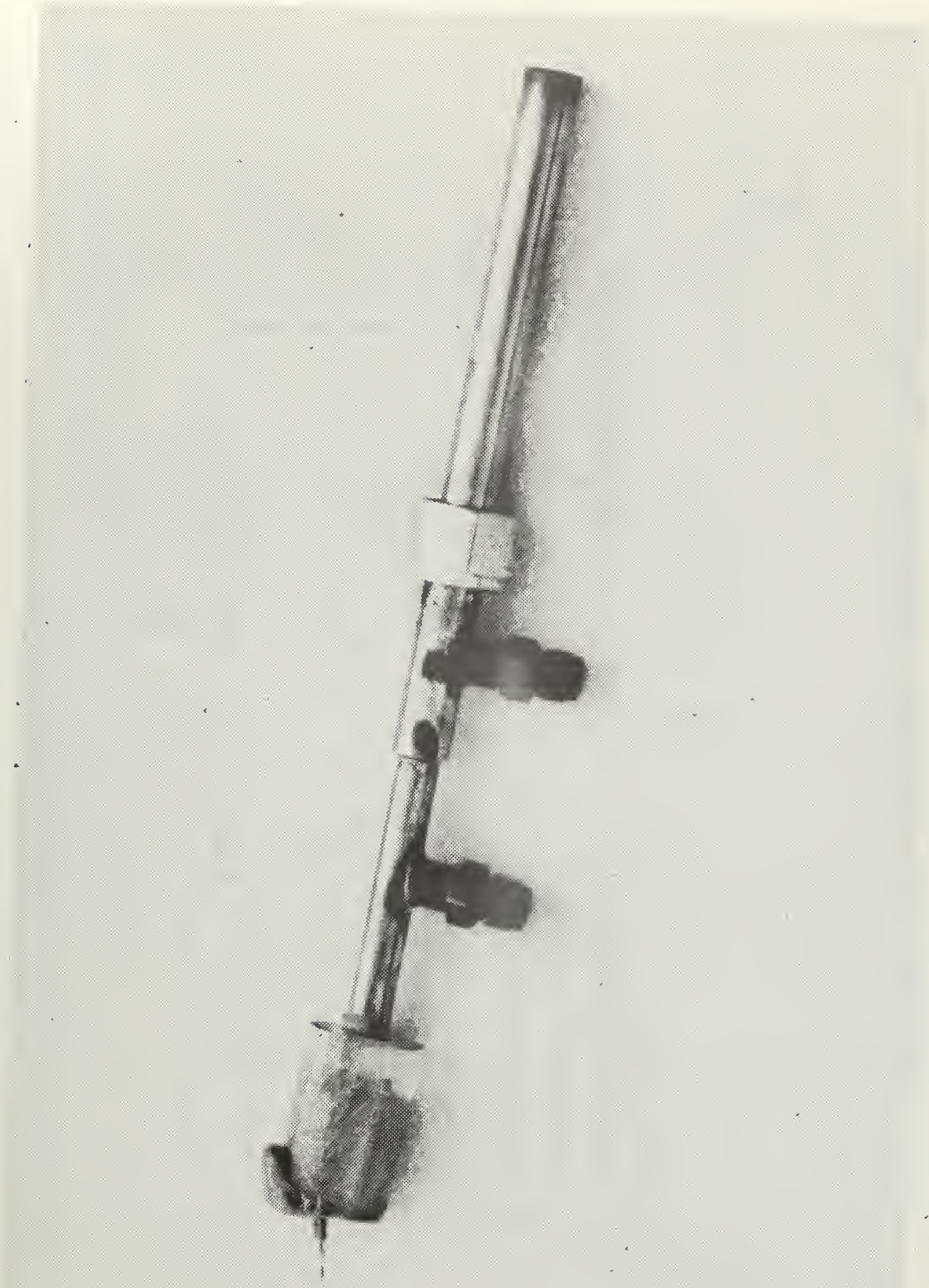

Figure 21. Igniter

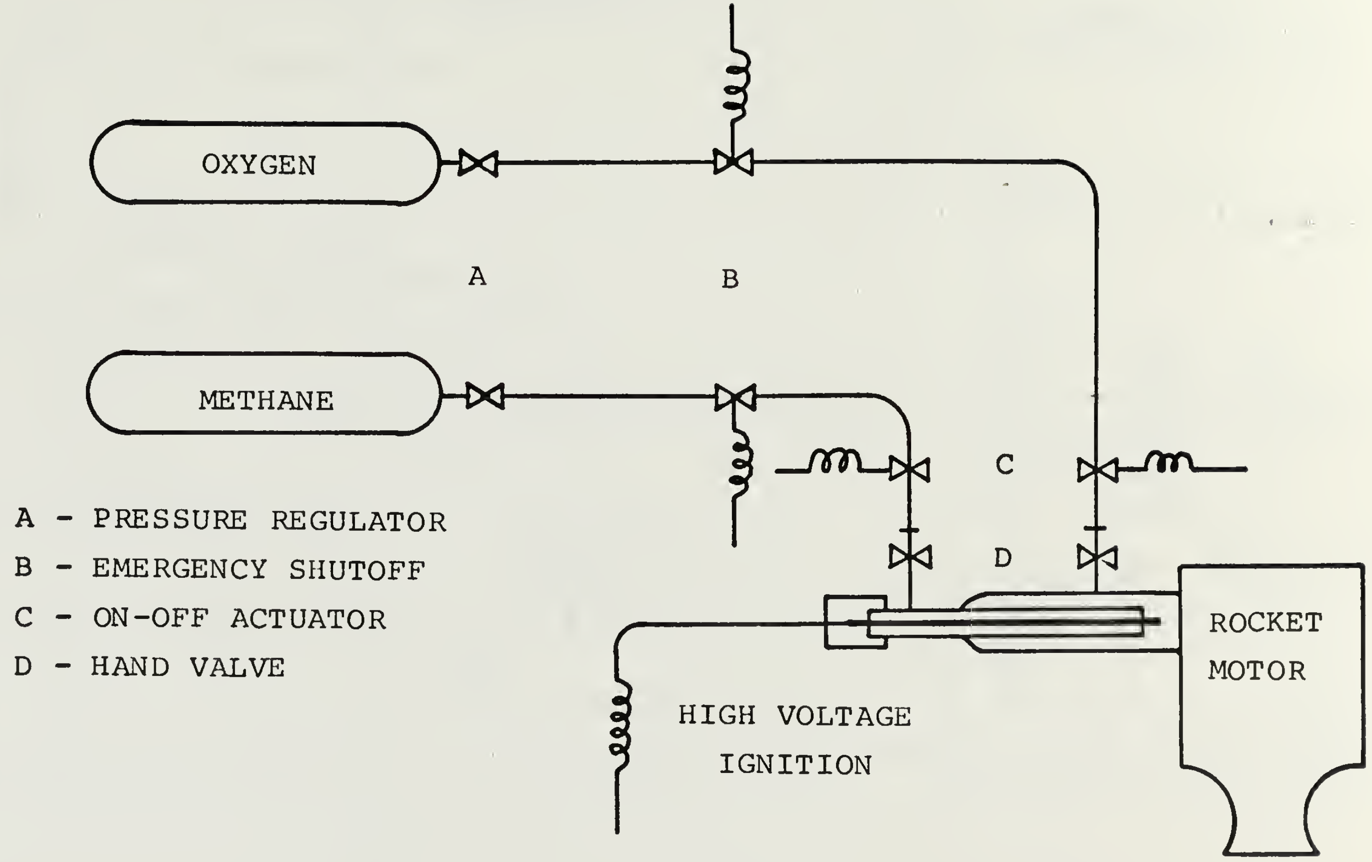

FIGURE 22. ROCKET IGNITION CONTROL

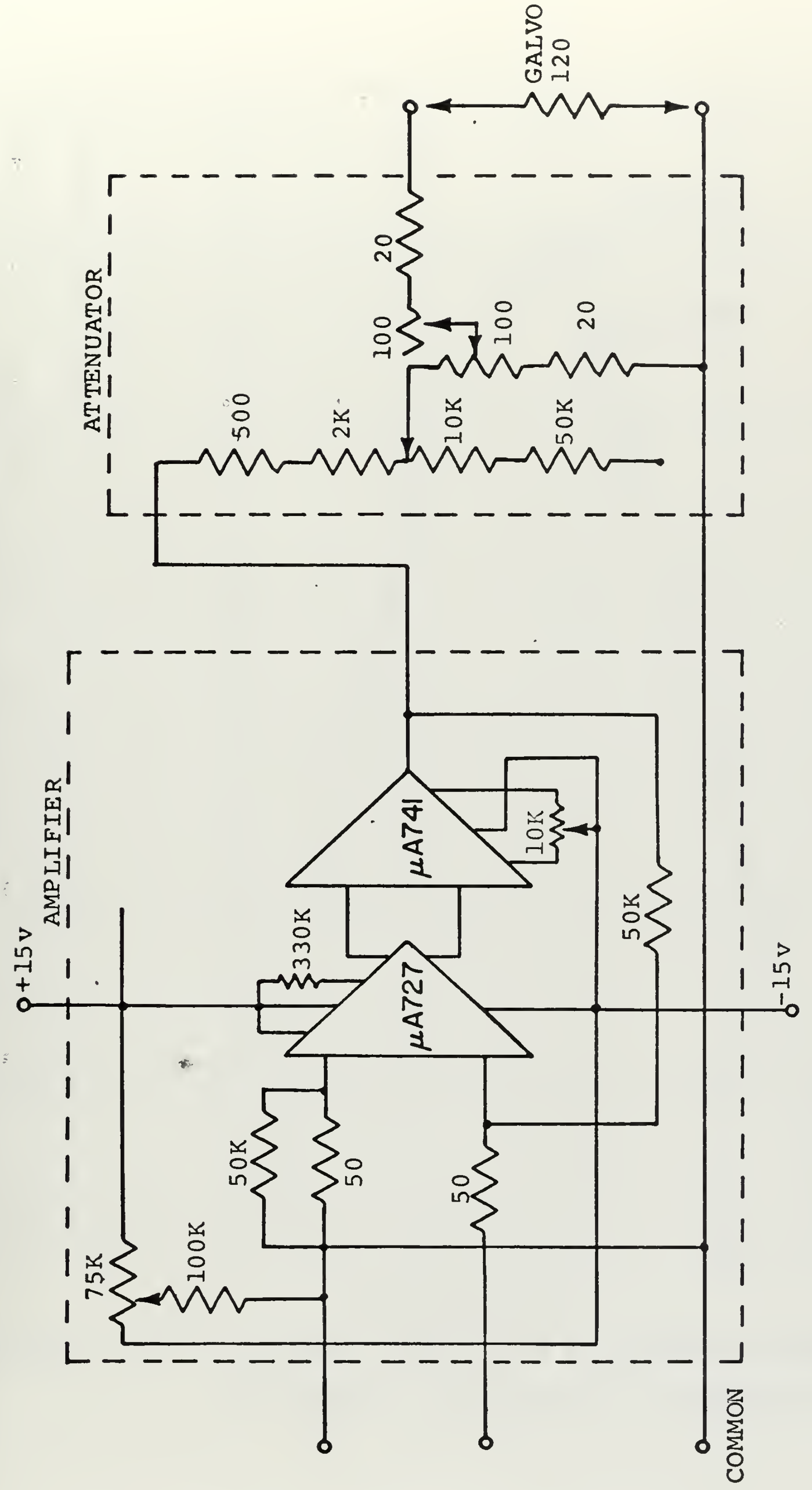

FIGURE 23. SIGNAL CONDITIONER

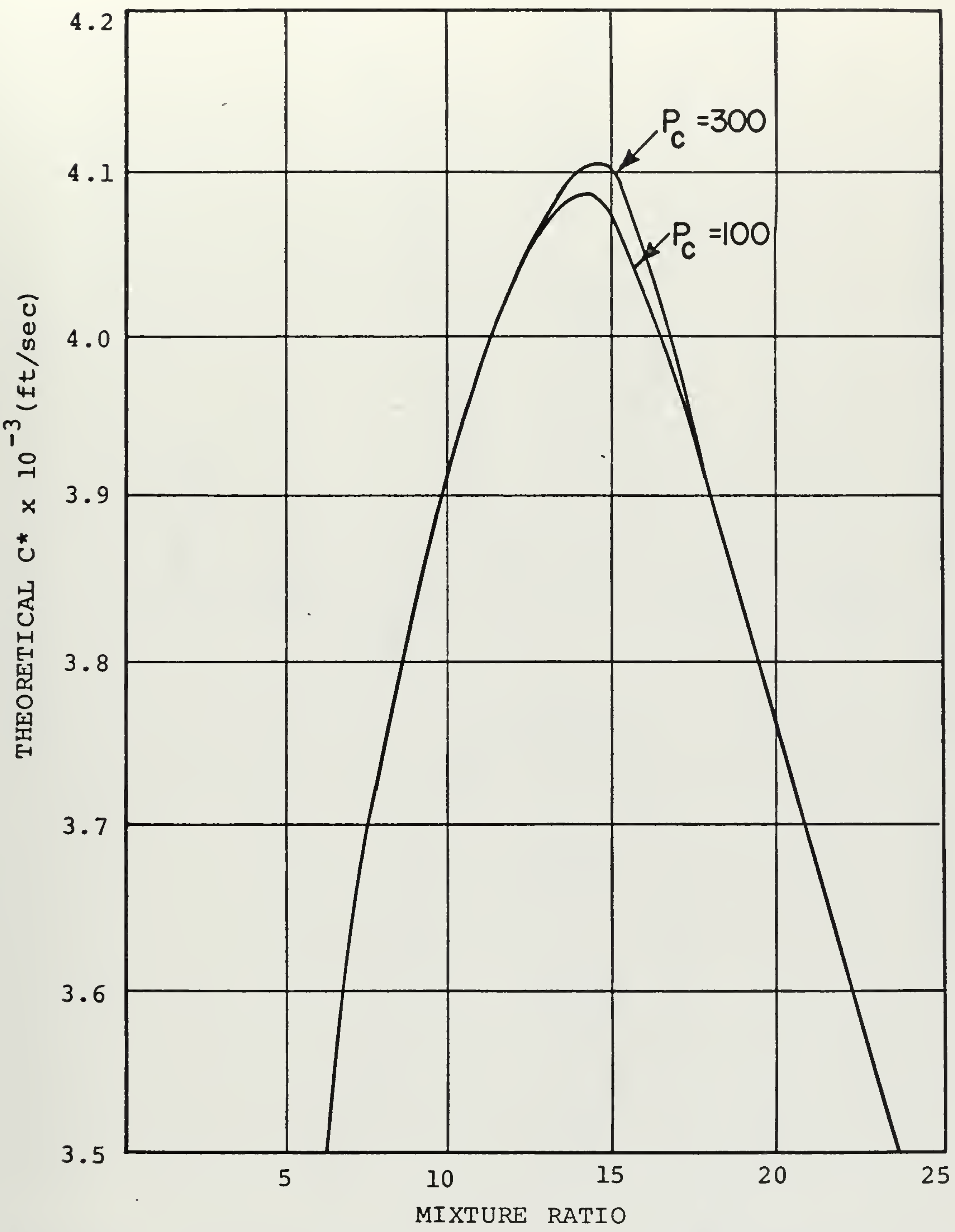

FIGURE 24. MIXTURE RATIO vs. CHARACTERISTIC EXHAUST VELOCITY (FROM REF. 18)

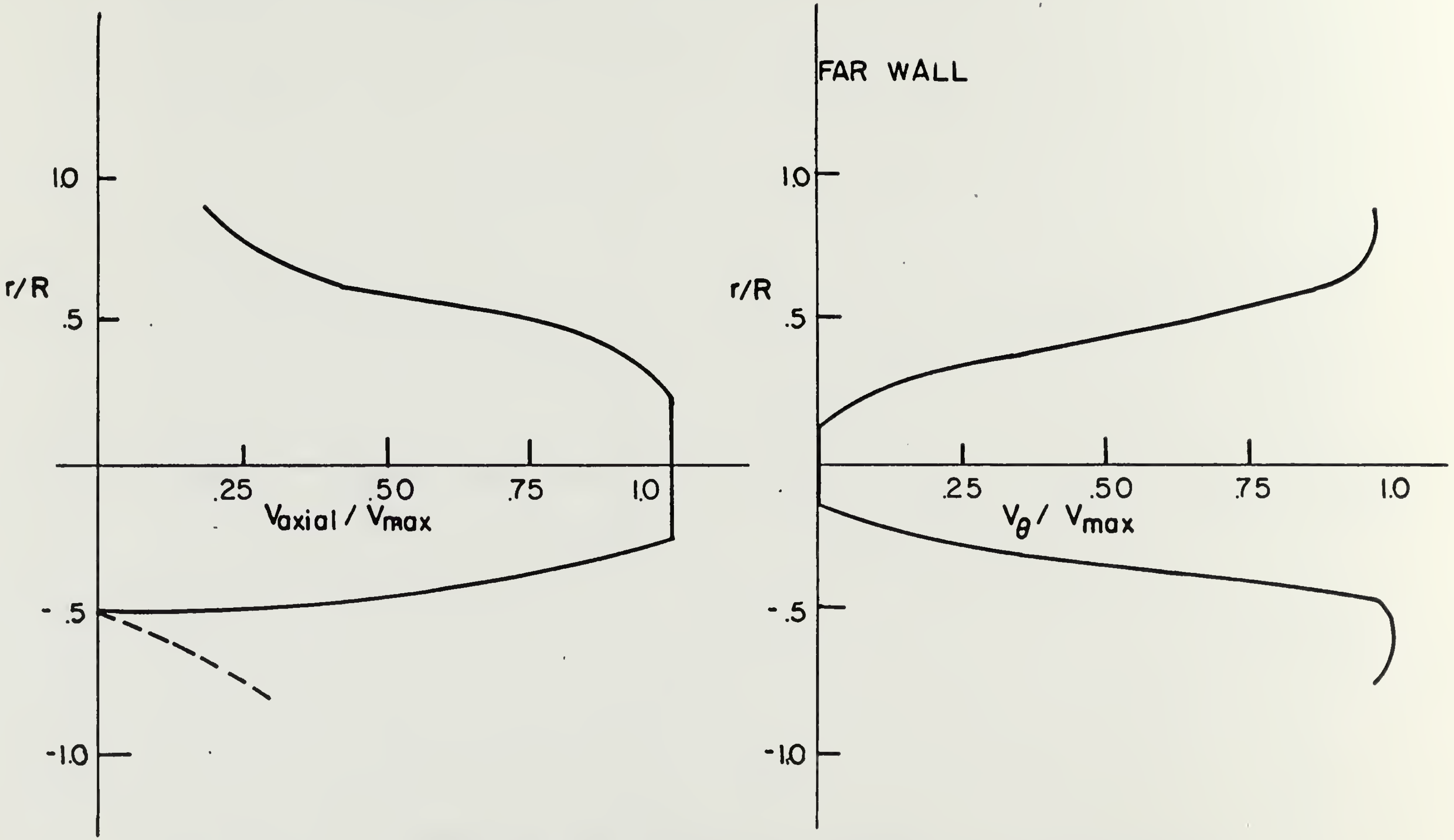

FIGURE 25. VELOCITY PROFILE - 20° INSERTS
22 % SECONDARY AIR

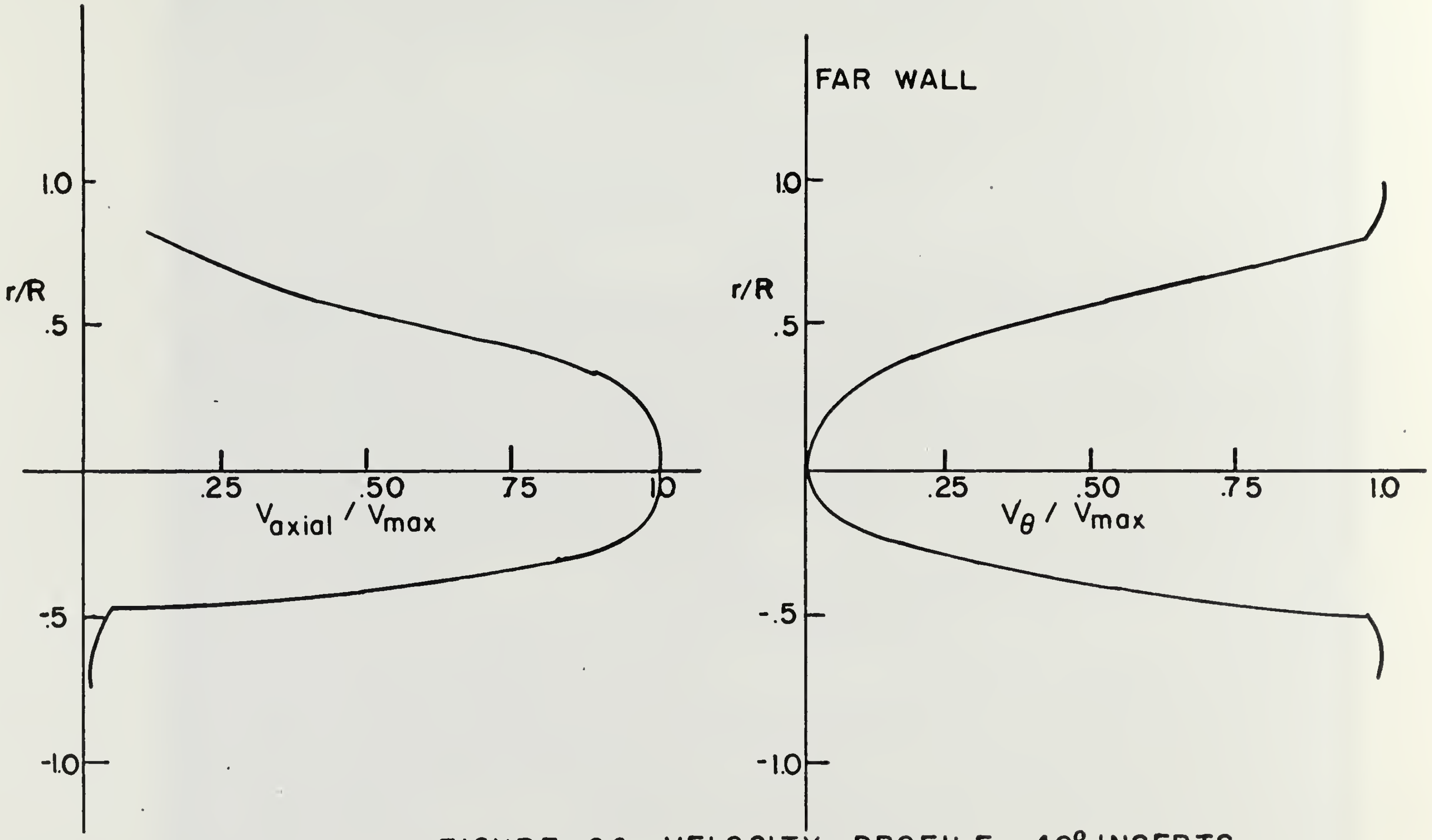

FIGURE 26. VELOCITY PROFILE - 40° INSERTS
22 % SECONDARY AIR

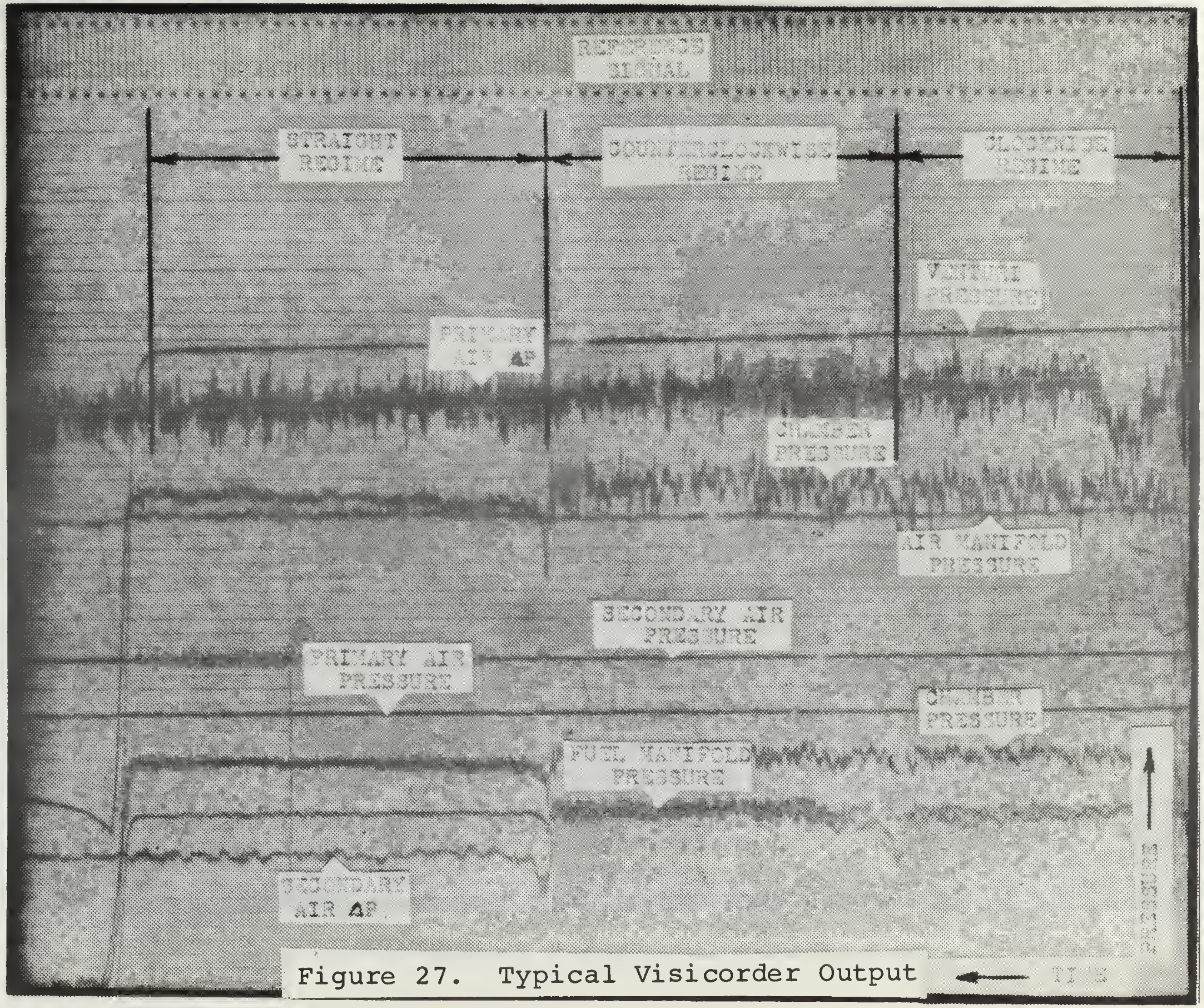

Figure 27. Typical Visicorder Output

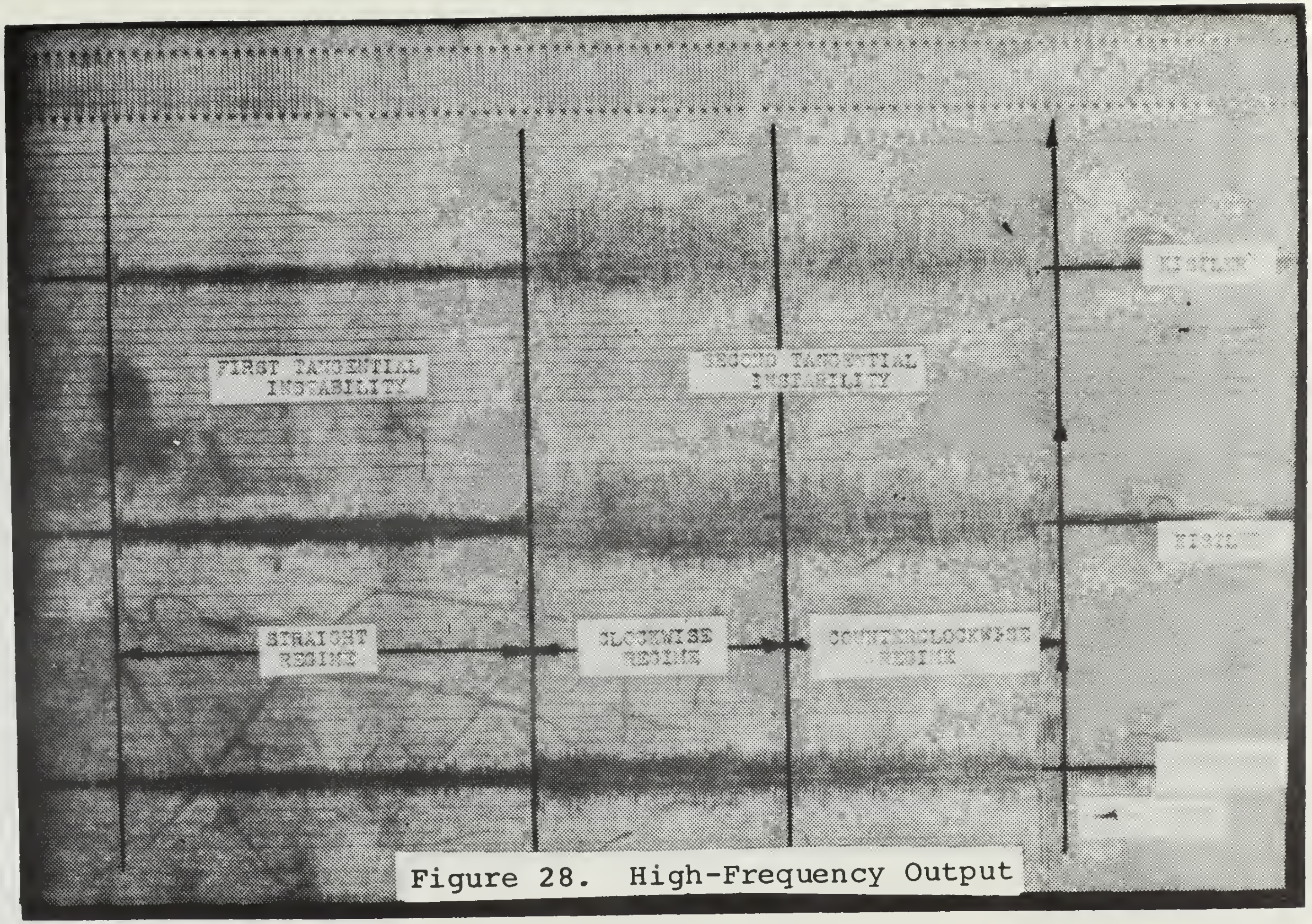

Figure 28. High-Frequency Output

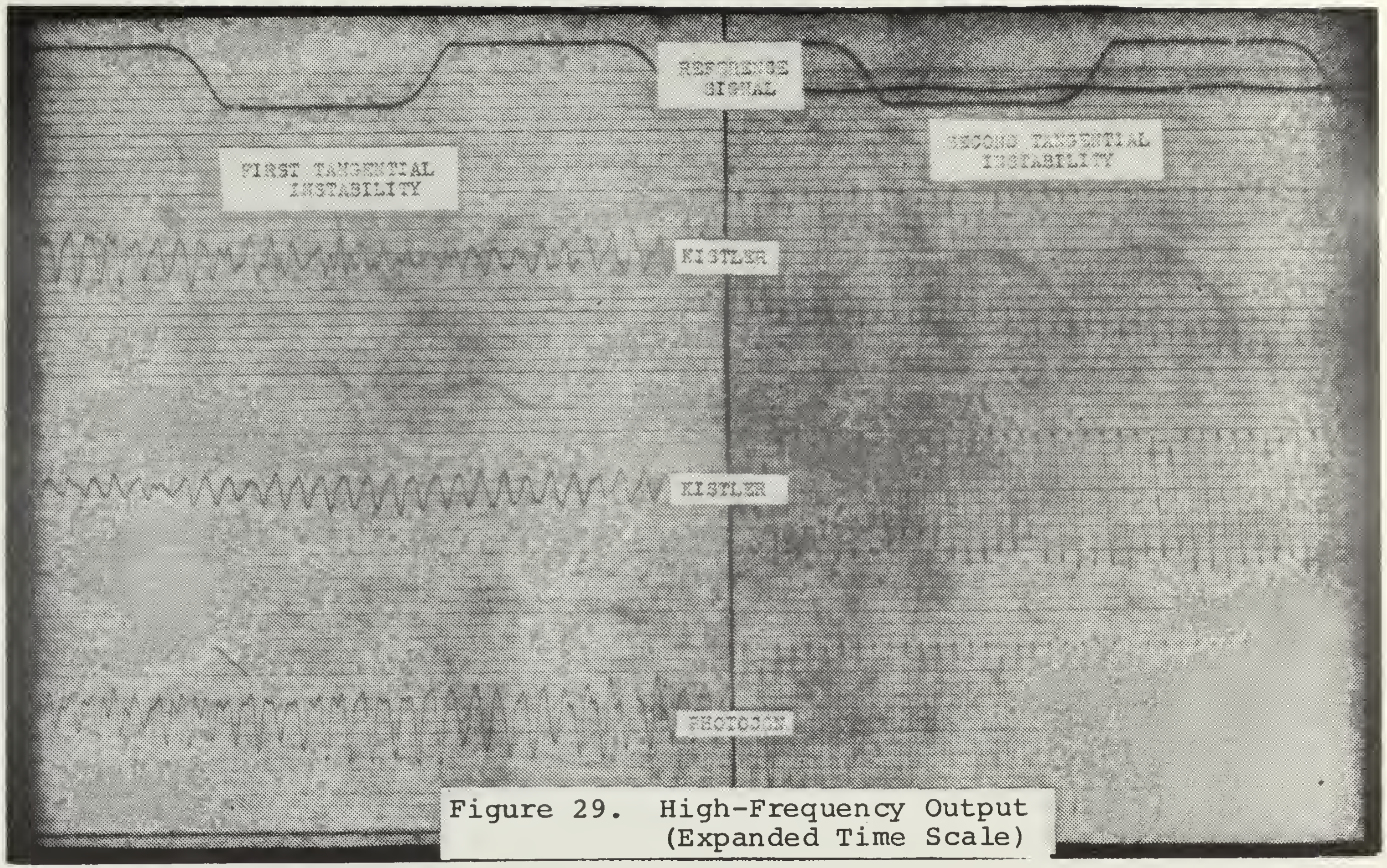

Figure 29. High-Frequency Output (Expanded Time Scale)

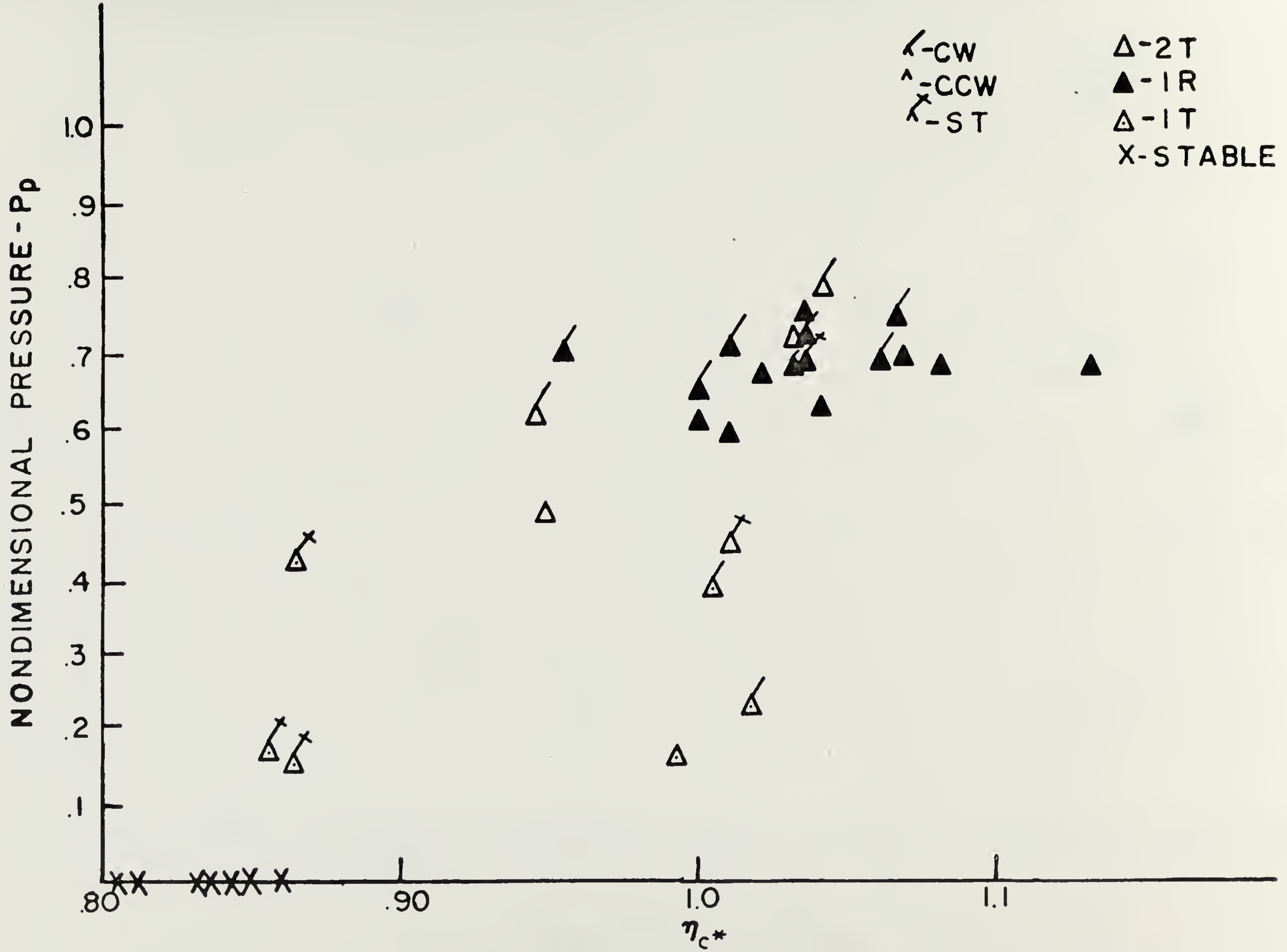

FIGURE 30. COMBUSTION EFFICIENCY vs. P_p

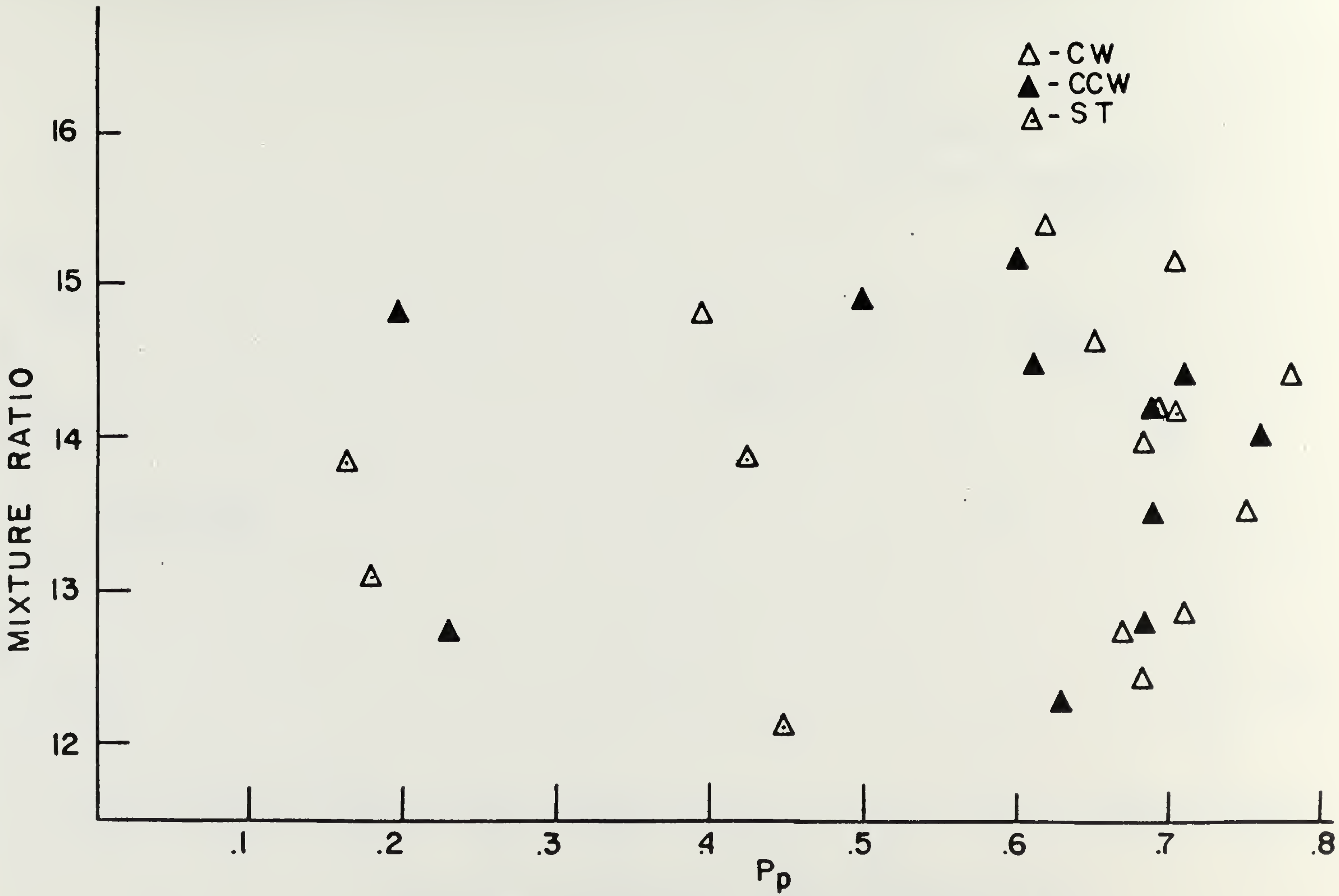

FIGURE 31. MIXTURE RATIO vs. P_p

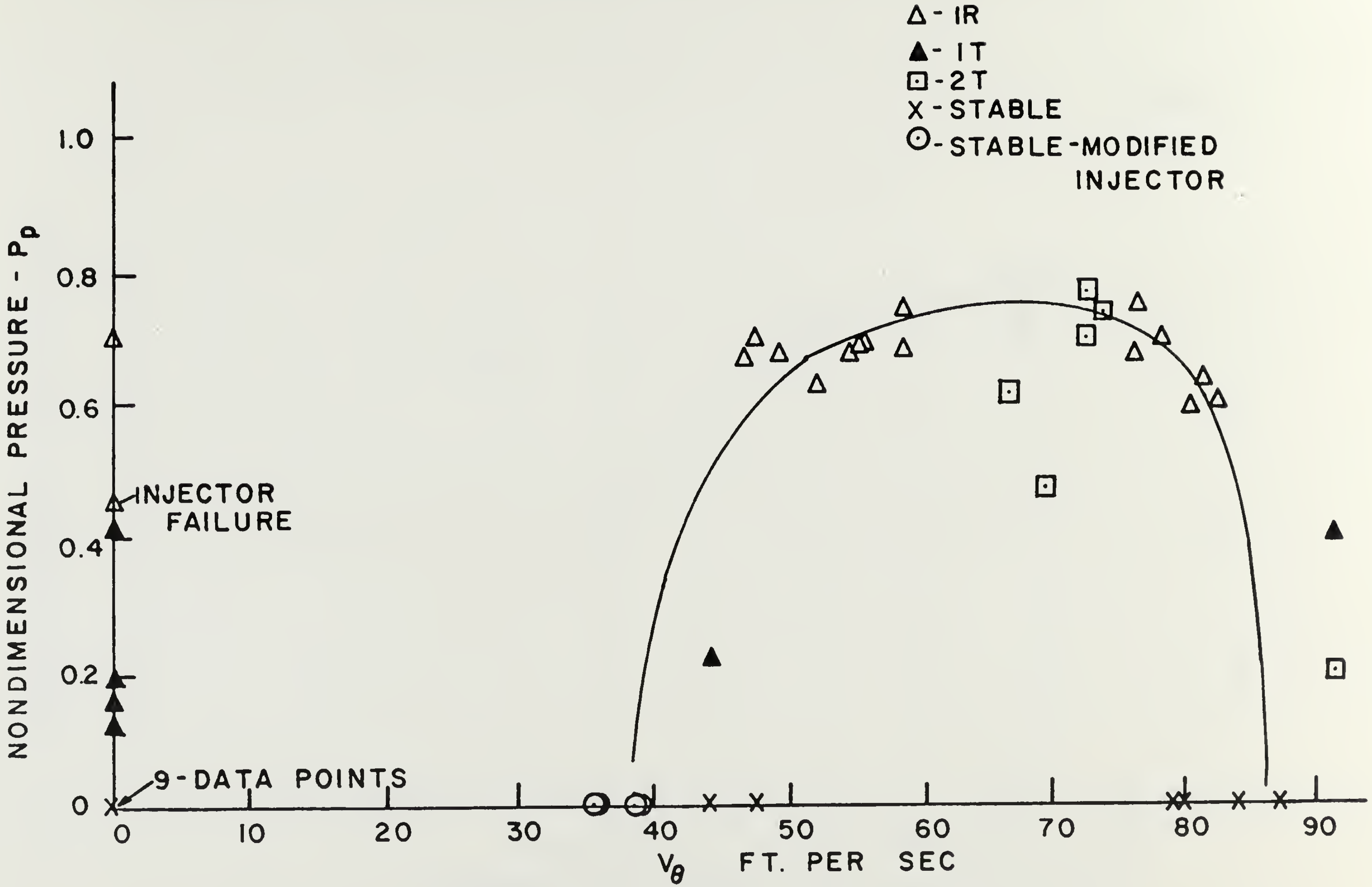

FIGURE 32. TANGENTIAL GAS VELOCITY vs. P_p

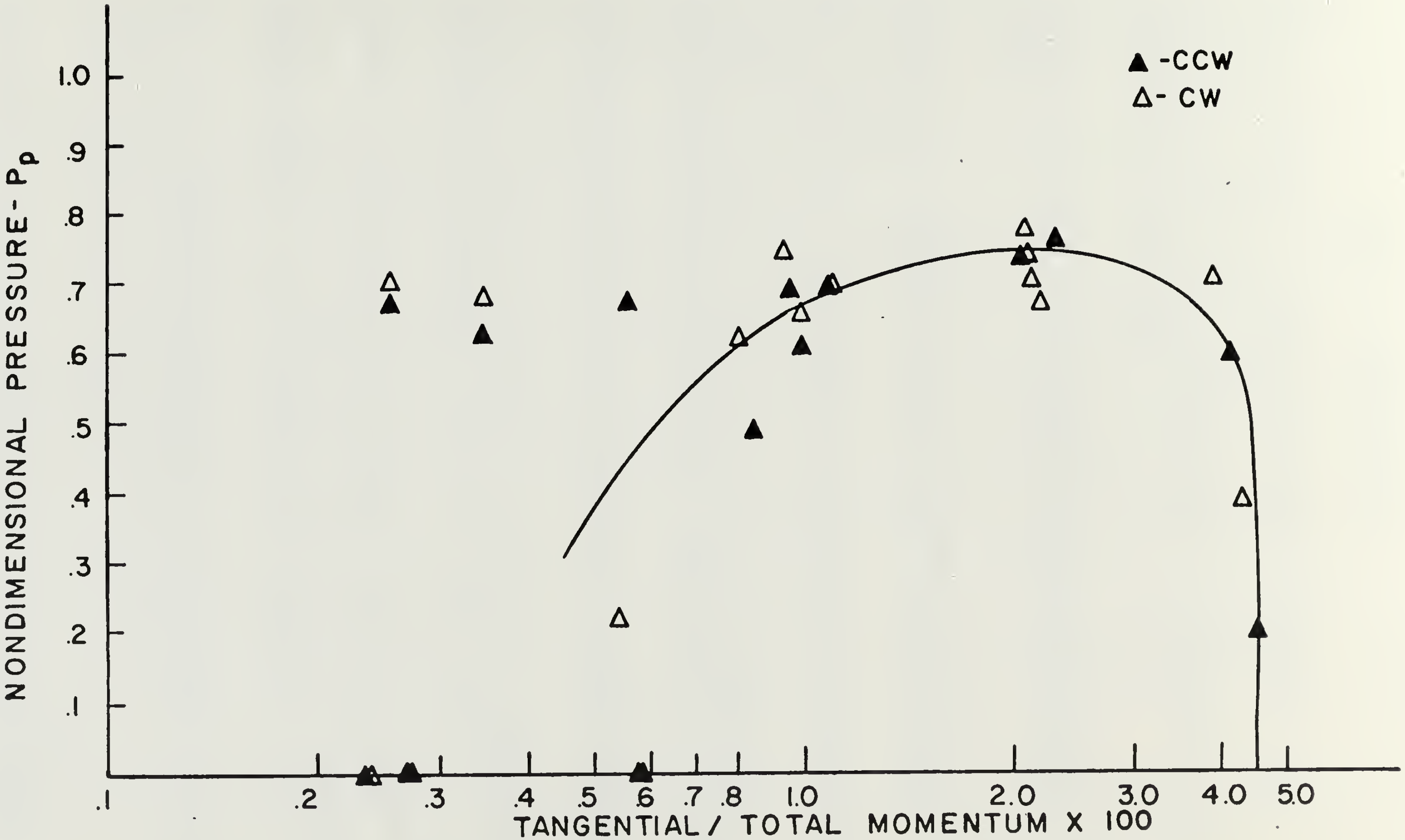

FIGURE 33. TANGENTIAL MOMENTUM vs. P_p

LIST OF REFERENCES

1. Sutton, George P., Rocket Propulsion Elements, 3rd Edition, John Wiley and Sons, Inc., 1963.

2. Weiss, Richard R., An Introduction to Combustion Instability in Liquid Propellant Rocket Engines, AFRPL-TR-66-150, 1966.

3. Strahle, Warren C., New Consideration on Causes for Combustion Instability in Liquid Propellant Rockets, "Combustion Science and Technology," Vol. 2, pp. 29-40, 1970.

4. Netzer, D. W., Investigation of Combustion Characteristics of a Bi-Phase Rocket, Ph.D. Thesis, Purdue University, 1968.

5. Priem, Richard J., Influence of Combustion Process on Stability, NASA TN D-2957, 1965.

6. Heidmann, Marcus F. and Wieber, Paul R., Analysis of n-Heptane Vaporization in Unstable Combustor with Traveling Transverse Oscillations, NASA TN D-3424, 1966.

7. Reardon, F. H., Crocco,L., Harrje, D. T., Velocity Effects in Transverse Mode Liquid Propellant Rocket Combustion Instability, A.I.A.A. Journal, Vol. 2, No. 9, 1964.

8. Heidmann, Marcus F. and Feiler, Charles E. Evaluation of Tangential Velocity Effects on Spinning Transverse Combustion Instability, NASA TN D-3406, 1966.

9. Heidmann, Marcus F., Oscillatory Combustion of a Liquid-Oxygen Jet with Gaseous Hydrogen, NASA TN D-2753.

10. Heidman, Marcus F., Oxygen-Jet Behavior During Combustion Instability in a Two Dimensional Combustor, NASA TN D-2725, 1965.

11. Kiel, J. A., An Investigation of the Effects of a Tangential Gas Velocity on Combustion Instability, Engineers Thesis, Naval Postgraduate School, 1969.

12. Raleigh, John W. S., The Theory of Sound, Vol. II, 2nd Ed., Dover Publications, 1945.

13. Priem, Richard J. and Guentert, Donald C., Combustion Instability Limits Determined by a Nonlinear Theory and a One-Dimensional Model, NASA TN D-1409, 1962.

14. Priem, Richard J. and Heidmann, Marcus F., Propellant Vaporization as a Design Criteria for Rocket Engine Combustion Chambers, NASA TR R-67, 1962.

15. Morse, P. M., Vibration and Sound, McGraw-Hill Book Company, Inc., 1958.

16. Smith, R. D. and Sprenger, P. F., Combustion Instability in Solid Propellant Rockets, 4th Symposium (International) on Combustion, 1952.

17. The American Society of Mechanical Engineers, Instruments and Apparatus, Chapter 4, Flow Measurement.

18. Scofield, M. P., A Generalized Thermo Chemistry Computer Program, Jet Propulsion Center, Purdue University, 1960.

19. Coates, R. L., Comment on Stability of Longitudinal Oscillations with Pressure and Velocity Coupling in a Solid Propellant Rocket, "Combustion Science and Technology," Vol. 3, p. 153, 1971.

20. Zinn, B. T. and Powell, E. A., Nonlinear Combustion Instability in Liquid Propellant Rocket Engines, 13th Symposium on Combustion, 1971.

21. Beltran, M. R., Breen, B. P., et al, Liquid Rocket Engine Combustion Instability Studies, AFRPL-TR-66-125, 1 July 1966.

INITIAL DISTRIBUTION LIST

		No. Copies
1.	Defense Documentation Center Cameron Station Alexandria, Virginia 22314	2
2.	Library, Code 0202 Naval Postgraduate School Monterey, California 93940	2
3.	Asst Professor D. W. Netzer Department of Aeronautics Naval Postgraduate School Monterey, California 93940	4
4.	R. W. Bell Chairman, Department of Aeronautics Naval Postgraduate School Monterey, California 93940	1
5.	Donald W. Avery Jr. 1007 Halsey Drive Monterey, California 93940	2

DOCUMENT CONTROL DATA - R & D

(Security classification of title, body of abstract and indexing annotation must be entered when the overall report is classified)

1. ORIGINATING ACTIVITY (Corporate author) Naval Postgraduate School Monterey, California 93940	2a. REPORT SECURITY CLASSIFICATION Unclassified 2b. GROUP

3. REPORT TITLE

THE EFFECT OF TANGENTIAL GAS VELOCITY
ON COMBUSTION INSTABILITY
IN A LIQUID-GAS COMBUSTOR

4. DESCRIPTIVE NOTES (Type of report and, inclusive dates)

Aeronautical Engineer; December 1971

5. AUTHOR(S) (First name, middle initial, last name)

Donald William Avery Jr.
Lieutenant Commander, United States Navy
B.S., Tufts University, 1963

6. REPORT DATE December 1971	7a. TOTAL NO. OF PAGES 84	7b. NO. OF REFS 20
8a. CONTRACT OR GRANT NO. b. PROJECT NO. c. d.	9a. ORIGINATOR'S REPORT NUMBER(S) 9b. OTHER REPORT NO(S) (Any other numbers that may be assigned this report)	

10. DISTRIBUTION STATEMENT

Approved for public release; distribution unlimited.

11. SUPPLEMENTARY NOTES	12. SPONSORING MILITARY ACTIVITY Naval Postgraduate School Monterey, California 93940

13. ABSTRACT

A small, uncooled liquid rocket motor was utilized to examine the effects of the magnitude and direction of a steady vortex velocity on combustion instability. The rocket operated on normal heptane and air, with air flow rates controllable to allow for various amounts of tangential momentum.

Results of this investigation indicated that an energy feedback mechanism, through tangential momentum, did exist for both tangential and radial modes of instability. It was further shown that limit values of tangential velocity did exist, for a particular combustor, above and below which instability did not occur.

KEY WORDS	LINK A		LINK B		LINK C	
	ROLE	WT	ROLE	WT	ROLE	WT
combustion instability rocket liquid propellant						

134497

Thesis
A976 Avery
c.1
The effect of tangential gas velocity on combustion instability in a liquid-gas combustor.

Thesis
A976 Avery 134497
c.1
The effect of tangential gas velocity on combustion instability in a liquid-gas combustor.

thesA976
The effect of tangential gas velocity on
3 2768 001 91087 0
DUDLEY KNOX LIBRARY